White Rose Research Online
eprints@whiterose.ac.uk
https://eprints.whiterose.ac.uk
Universities of Leeds, Sheffield and York

Deposited via The University of Sheffield.

White Rose Research Online URL for this paper:
https://eprints.whiterose.ac.uk/id/eprint/243340/

Version: Published Version

Article:
Szewczyk, K.M., Iglesias, D.P. and Panić, O. (2026) A search for circumstellar gas in pre-main-sequence debris discs using absorption spectroscopy. Monthly Notices of the Royal Astronomical Society, 550 (4). stag1309. ISSN: 0035-8711

https://doi.org/10.1093/mnras/stag1309

Reuse
This article is distributed under the terms of the Creative Commons Attribution (CC BY) licence. This licence allows you to distribute, remix, tweak, and build upon the work, even commercially, as long as you credit the authors for the original work. More information and the full terms of the licence here:
https://creativecommons.org/licenses/

Takedown
If you consider content in White Rose Research Online to be in breach of UK law, please notify us by emailing eprints@whiterose.ac.uk including the URL of the record and the reason for the withdrawal request.

UNIVERSITY OF LEEDS
University of Sheffield
UNIVERSITY of York

Monthly Notices
of the
ROYAL ASTRONOMICAL SOCIETY

MNRAS **550**, 1–20 (2026)
Advance Access publication 2026 July 10

https://doi.org/10.1093/mnras/stag1309

A search for circumstellar gas in pre-main-sequence debris discs using absorption spectroscopy

Karolina M. Szewczyk ,[1★] D. P. Iglesias [1,2] and O. Panić [1]
[1]School of Physics & Astronomy, University of Leeds, Sir William Henry Bragg Building, Woodhouse Lane, Leeds LS2 9JT, UK
[2]Astrophysics Research Cluster, School of Mathematical and Physical Sciences, The University of Sheffield, Hounsfield Road, Sheffield S3 7RH, UK

Accepted 2026 June 29. Received 2026 June 26; in original form 2026 March 16

ABSTRACT

Gas in debris discs is thought to be either inherited from the protoplanetary stage or released from the solid, rocky content of planetesimal belts. Its presence can impact planetary atmospheres and their potential for habitability, which stresses the need to ascertain its origin and composition. Most detections to date are around main-sequence stars, with only a few gas-bearing debris discs identified around pre-main-sequence stars, mainly through millimetre CO line searches. We investigate narrow gas absorption features superimposed on the photospheric Ca II K & H and Na I D1 & D2 lines in a sample of 125 pre-main sequence and 5 relatively young (< 17 Myr) stars. All stars are associated with IR excess emission indicative of the presence of a debris disc. By comparing their residual spectra (photosphere-subtracted) to those of nearby stars, interstellar cloud velocities, and stellar radial velocities, we test whether interstellar absorption is the culprit and ascertain the circumstellar gas origin. Using these methods, out of the 130 targets, we identified two new gas-bearing debris discs: TYC 7879-1373-1, which exhibits stable absorption, and HIP 30414, which shows variable gas absorption features linked likely to ongoing accretion. Both these systems are pre-main-sequence stars younger than 5 Myr. TYC 6822-283-1 has absorption features of inconclusive origin. This study increases the number of currently known very young (< 10 Myr) debris discs with circumstellar gas to eight, paving the path to future systematic studies of objects caught in transition from protoplanetary to debris disc stages.

Key words: protoplanetary discs – circumstellar matter – planetary systems – stars: pre-main-sequence.

1 INTRODUCTION

The detection of gas in debris discs remains relatively rare, although recent discoveries suggest it may not be as uncommon as once thought. Debris discs are circumstellar discs of dust and planetesimals typically found around main-sequence (MS) stars (although not limited to them, D. Veras et al. 2020). Protoplanetary discs, which are the earlier evolutionary stage, are gas-rich objects formed from the initial molecular cloud collapse, whose mass is dominated by gas, with gas-to-dust mass ratio of ∼100 (S.-I. Inutsuka et al. 2023). During the transition from protoplanetary to debris phase, most of the gas (and dust) is removed through a combination of photoevaporation, accretion onto the star, and planet formation, typically within ∼3–11 Myr but depending on the stellar mass of the parent star (K. E. Haisch, E. A. Lada & C. J. Lada 2001; J. Hernández et al. 2007; Á. Ribas, H. Bouy & B. Merín 2015). The primordial disc becomes depleted, leaving behind larger bodies, which will continue to undergo collisions, generating dust that sustains the observed debris disc (M. C. Wyatt 2008). Unlike protoplanetary discs, debris discs generally do not contain much gas and used to be considered devoid of it (e.g. in D. E. Backman & F. Paresce 1993). However, the discovery of gas in the debris disc of β Pic (L. M. Hobbs et al. 1985) challenged this belief and initiated the efforts to understand the physical mechanisms that allow the gas to be present in the later stages of planetary system evolution. To date, the debris disc around β Pic contains the widest range of detected gas species, including Ca, Na, CO, C, O, Fe, and many more (for a complete list see D. Iglesias et al. 2025). This transient gas has since been shown to be primarily produced by exocomets – minor bodies that sublimate as they approach the star (W. R. F. Dent et al. 2014; Q. Kral et al. 2016).

Gas has now been detected in nearly 50 debris discs, with ages ranging from ∼2 to ∼1500 Myr (1–3 Myr NO Lup, J. B. Lovell et al. 2021a; 1–2 Gyr η Crv, S. Marino et al. 2017) through either emission (e.g. J. Lieman-Sifry et al. 2016; A. Moór et al. 2017; S. Hales et al. 2022; G. Cataldi et al. 2023) or absorption (e.g. A. M. Lagrange-Henri et al. 1990; S. L. Montgomery & B. Y. Welsh 2012; D. Iglesias et al. 2018; D. P. Iglesias et al. 2019), summarized in Fig. 1. These systems span a wide range of CO abundances. Some, like β Pic, only contain low levels of CO, while others show CO gas masses comparable to those in protoplanetary discs. While emission studies allow for direct observations of gas, identifying it through absorption requires less telescope time (D. Iglesias et al. 2018), hence is a time-effective method. The gas species

★ E-mail: py19k2ms@leeds.ac.uk

© The Author(s) 2026.
Published by Oxford University Press on behalf of Royal Astronomical Society. This is an Open Access article distributed under the terms of the Creative Commons Attribution License (https://creativecommons.org/licenses/by/4.0/), which permits unrestricted reuse, distribution, and reproduction in any medium, provided the original work is properly cited.

Downloaded from https://academic.oup.com/mnras/article/550/4/stag1309/8732235 by guest on 31 July 2026

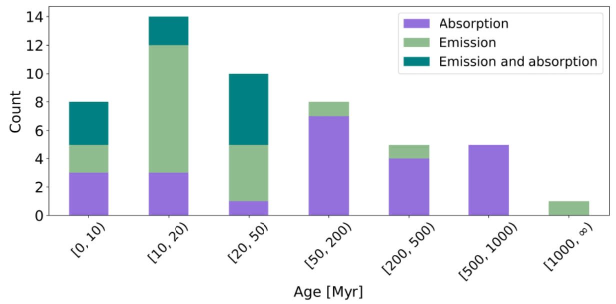

Figure 1. Histogram of all gas detections in debris discs through either emission or absorption, divided into bins of age, including HIP 30414 and TYC 7879-1373-1. Objects with gas emission and their ages were adopted from K. M. Szewczyk et al. (2025) (Table A1), based on the data from J. B. Lovell et al. (2021a), J. M. Miley et al. (2018), I. Rebollido et al. (2022), L. Matrà et al. (2019), J. Lieman-Sifry et al. (2016), T. Schneiderman et al. (2021), S. Hales et al. (2022), A. Moór et al. (2017), S. Marino et al. (2016), W. R. F. Dent et al. (2014), P. Riviere-Marichalar et al. (2014), A. Moór et al. (2019), Á. Kóspál et al. (2013), J. Péricaud et al. (2017), L. Matrà et al. (2017), and S. Marino et al. (2017). We additionally included HD 9985, HD 145101, HD 152989, HD 155853, and HD 170116 from A. Moór et al. (2025). Objects with gas absorption and their ages used in this figure were adopted from D. Iglesias (2020) (Table 1.1), based on data from C. H. Chen & M. Jura (2003), A. M. Lagrange-Henri et al. (1990), H. A. Abt & K. I. Moyd (1973), B. Y. Welsh & S. Montgomery (2013), P. Koubsky et al. (1993), D. Iglesias et al. (2018), D. P. Iglesias et al. (2019), B. Y. Welsh et al. (1998), B. Y. Welsh & S. L. Montgomery (2015), S. L. Montgomery & B. Y. Welsh (2012), B. Y. Welsh & S. L. Montgomery (2018).

commonly detected differ between the two methods. CO and C I are primarily observed in emission, and CO is currently the only molecule detected in the millimetre regime (e.g. J. Lieman-Sifry et al. 2016; Q. Kral et al. 2020b; J. B. Lovell et al. 2021a; S. Hales et al. 2022); Ca II K & H and Na I D1 & D2 doublets are the most commonly used in absorption spectroscopy (e.g. B. Y. Welsh & S. L. Montgomery 2015; A. S. Hales et al. 2017; D. Iglesias et al. 2018), although CO and C I have also been detected in absorption in a few systems (e.g. A. Roberge et al. 2000; A. Brennan et al. 2024). The wavelengths probed by these two methods also differ. Emission studies typically target sub-millimetre and millimetre transitions of cold molecular gas using radio interferometers, while absorption studies detect ultraviolet and optical absorption lines seen against the stellar continuum. Nonetheless, both methods are crucial for our understanding of the evolution of debris discs and the processes that shape planetary systems.

Over the past decade, numerous studies have searched for gas in debris discs by analysing Ca II absorption lines. A. S. Hales et al. (2017) examined spectra of 16 debris disc host stars and found four stars showing narrow Ca II or Na I D absorption features. However, a comparison with stellar radial velocities, interstellar clouds, column densities, and neighbouring stars suggested that only one system, HD 110058, hosted circumstellar gas. Similarly, in a survey of 301 debris discs, 23 of which exhibited narrow absorption features, D. Iglesias et al. (2018) identified three systems with circumstellar gas: HD 110058, with stable absorption, as well as HR 4796 and c Aql, with variable absorption features.

Two main gas origin scenarios have been proposed for debris discs: primordial and secondary. In case of CO-poor discs, like β Pic, the origin of the gas is well established as secondary – produced within the debris disc, in a similar manner to dust, through, e.g. collisions or sublimation of planetesimals (Q. Kral et al. 2017; A. M. Hughes, G. Duchêne & B. C. Matthews 2018; Q. Kral et al. 2019). In these systems, the gas has to be of secondary origin, as the low CO levels must be continuously replenished, since the CO is rapidly photodissociated by the interstellar radiation field on a time-scale of ~130 yr when unshielded (A. N. Heays, A. D. Bosman & E. F. van Dishoeck 2017; S. Marino et al. 2022), so any primordial reservoir would long have been destroyed. Less is known in the case of CO-rich debris discs, in which both origin scenarios have been proposed. In the primordial scenario, the CO is a remnant of the protoplanetary disc, surviving from the initial collapse of the molecular cloud (M. C. Wyatt et al. 2015; R. Nakatani et al. 2021; G. V. Smirnov-Pinchukov et al. 2022). Most gas-bearing debris discs have been found around young ($\lesssim$40 Myr), A-type stars (A. M. Hughes et al. 2018, see also Fig. 1), supporting the primordial gas origin as these stars may be more likely to retain circumstellar gas from earlier evolutionary stages (R. Nakatani et al. 2021). In pre-MS A-type stars, X-ray radiation is weaker than in low-mass stars, while far-ultraviolet (FUV) radiation is the dominant photoevaporation mechanism. However, grain growth may inhibit FUV photoevaporation, potentially allowing gas to persist into the debris stage (R. Nakatani et al. 2021). In the absence of small dust grains, extreme-ultraviolet (EUV) radiation also becomes inefficient, allowing some of the gas to persist into the debris phase, where it may influence system dynamics (R. Nakatani et al. 2023). Detections around lower mass stars are indeed rarer (M. C. Wyatt et al. 2015), perhaps due to their stronger X-ray and FUV radiation driving more efficient photoevaporation. While CO in older debris discs, such as the 440 Myr Fomalhaut, is most likely secondary (L. Matrà et al. 2017), the youngest systems may still retain primordial gas.

Very few gas-bearing debris discs have been found around pre-MS stars, particularly those younger than ~10 Myr. Systems such as NO Lup (1–3 Myr, J. B. Lovell et al. 2021b), HD 44892 (2.1 Myr, K. M. Szewczyk et al. 2025), and HD 141569 (5 Myr, J. M. Miley et al. 2018) remain rare, although the gas in NO Lup is suspected to be wind-driven rather than from a disc. HD 44892 is a pre-MS A-type star, also known as HIP 30414, and a part of the sample we studied – we report the first evidence of gas absorption towards this disc in later sections. Targeting such young candidates is crucial for probing the poorly understood transitional stage from protoplanetary to debris discs, as it allows us to trace how the gas evolves in the first few million years after disc dispersal and how it may influence early planet formation and system architecture.

The origin of gas in the CO-rich debris discs is still not fully understood. While their dust masses are more typical of debris discs, their CO gas masses can be of similar magnitude to those of protoplanetary discs. J. Péricaud et al. (2017) first introduced the term'hybrid discs' for these systems, defining them as having gas of primordial origin but secondary dust. However, since then, some studies have shown that secondary processes, such as CO release from colliding or sublimating planetesimals, may also produce the high CO gas masses observed (e.g. Q. Kral et al. 2017; Q. Kral et al. 2019), challenging the primordial gas interpretation. As the CO gas origin in these systems remains uncertain, we adopt the term'hybrid disc candidates' only for the candidates identified by D. P. Iglesias et al. (2023a), in line with their classification and terminology. The youngest of CO-bearing debris discs are key for understanding how long gas can persist and influence planet formation – while giant planets are expected to form during the protoplanetary phase, terrestrial planet formation may continue in the debris stage and be shaped by the presence of gas

Downloaded from https://academic.oup.com/mnras/article/550/4/stag1309/8732235 by guest on 31 July 2026

(Q. Kral, J. Davoult & B. Charnay 2020a). HD 141569 is a well-studied example of a CO-rich disc ('hybrid disc' in D. P. Iglesias et al. 2023a), with a CO gas mass comparable to protoplanetary discs but a dust mass more typical of debris discs. Based on similarities in fractional IR excess to HD 141569, D. P. Iglesias et al. (2023a) identified 17 very young objects as'hybrid disc candidates'. Our study builds upon their work by searching for new detections of circumstellar gas in both their'hybrid candidates' and debris disc systems (all < 17 Myr), for a total sample of 130 targets.

2 SAMPLE SELECTION, OBSERVATIONS, AND DATA REDUCTION

2.1 Sample selection

Studying pre-MS stars is key to understanding the transition from protoplanetary to debris discs. D. P. Iglesias et al. (2023a) conducted a large spectroscopic survey of intermediate-mass (1.5 – 3.5 $M_\odot$) pre-MS stars using X-Shooter on the Very Large Telescope (VLT), aiming to identify new young stars exhibiting disc excess. From their full sample, they identified 135 objects showing infrared (IR) excess at 12 μm, indicative of warm dust in a circumstellar disc. These systems were classified using their fractional 12 μm excess, with protoplanetary discs defined as those with $\frac{F_{12\mu m}}{F_*} > 25$ and debris discs with $\frac{F_{12\mu m}}{F_*} < 2$ (M. C. Wyatt et al. 2015; D. P. Iglesias et al. 2023a).

From the 135 sources identified by D. P. Iglesias et al. (2023a), we exclude the five systems whose excesses fall in the protoplanetary disc regime, leaving a working sample of 130 objects. Of these, 22 had suitable archival high-resolution spectra, while for the remaining 108 we obtained new Ultraviolet and Visual Echelle Spectrograph (UVES; H. Dekker et al. 2000) observations. The sample spans stellar masses of 1.51 –3.46 $M_\odot$, distances of 54.8 –292.0 pc, and ages between 1.61 and 16.94 Myr. Based on their 12 μm fractional excesses, 113 of the 130 stars fall within the debris disc regime, while 17 are found in the region between debris and protoplanetary discs, classified as'hybrid disc candidates' in D. P. Iglesias et al. (2023a) based on M. C. Wyatt et al. (2015). The sample consists of B-, A-, and F-type stars, which have fewer and broader spectral lines (S. Reffert et al. 2015), making narrow absorption features easier to identify. A-type stars in particular have been found to host gas-bearing debris discs more frequently than other spectral types, with ∼70 per cent of known detections occurring around them (A. Moór et al. 2017). Moreover, given their young ages (<17 Myr), all 130 systems, whether already debris or caught in the transition from protoplanetary to debris disc stages, are plausible hosts of circumstellar gas, which may be primordial, secondary, or mixed, as most detections are around younger debris disc systems (see Fig. 1).

2.2 Observations

We obtained the high-resolution spectra for the 108 stars in our sample, which did not have suitable archival data available using UVES at the VLT in Cerro Paranal, Chile. Observations were carried out between May 2022 and February 2024 (ESO periods 109, 110 and 112).[1] Spectra were obtained using the 0.6' slit and the dichroic DIC1 set-up centred at 390 nm and 580 nm, respectively, for the BLUE and RED arms. The remaining 22 stars already had high-resolution (R > 40000) spectroscopic observations in the ESO archive[2] from spectrographs such as UVES, HARPS (M. Mayor et al. 2003), and FEROS (A. Kaufer et al. 1999), at the La Silla Observatory. Therefore, for these stars, we used their available archival spectra instead of obtaining new observations. Observations of our sample are summarized in Table B1.

In addition, for each star in the sample, we identified comparison stars based on their nearby location on the sky (see Section 3.2) and for these we searched the ESO archive for high-resolution spectroscopic data. We retrieved optical spectra from UVES, FEROS, or HARPS spectrographs of stars within a maximum of 5° of our targets, resulting in a sample of 134 comparison stars. Wherever possible, we prioritized stars with similar distances from the Sun, the smallest angular separation from the target, and with B, A, or F spectral types, since narrow absorption features are more easily identified in these stellar types. Where we did not find suitable comparison stars in the ESO archive, we conducted additional observations[3] with UVES of 38 stars using the same observing set-up to ensure that each target had at least one well-suited comparison star, ideally within 1° separation. These additional observations are listed in Table B2.

2.3 Data reduction

All spectra of both science and comparison stars have been reduced with the data reduction software corresponding to each instrument. We reduced our UVES observations using the `EsoReflex` pipeline (W. Freudling et al. 2013) version 2.11.5. We applied a barycentric radial velocity correction to all UVES spectra a posteriori, as this is not included in the reduction pipeline. This is important for the determination of the radial velocity of the features and, thus, their diagnostic. For the RED arm spectra, in the case of UVES, and where pertinent, for the HARPS and FEROS data, we used Molecfit (W. Kausch et al. 2015; A. Smette et al. 2015) to correct for tellurics. The red wavelengths are highly contaminated by telluric lines due to mainly water vapour, O_2, and O_3 in the Earth's atmosphere. In particular, the Na I doublet is significantly affected by telluric lines contamination and, therefore, it is crucial to eliminate these lines when performing the analysis of the sodium lines.

3 METHODS

3.1 Identifying narrow absorption features

Gas detected through absorption spectroscopy does not necessarily originate from a circumstellar disc. Such features can arise from any gas in the line of sight between the observer and the star (D. Iglesias et al. 2018), including both the interstellar medium (ISM) clouds and circumstellar material. Determining the origin of these features is therefore crucial. We searched for narrow absorption features in the Ca II K & H (at 3933.663 Å & 3968.469 Å) and Na I D1 & D2 (at 5895.924 Å & 5889.950 Å) lines, which are superimposed on the star's broad photospheric absorption profiles. These additional components are far narrower than the stellar lines in early-type stars, typically only a

[1]ESO programmes 109.23K8.001, 110.23YZ.001, and 112.262P.001. PI: Iglesias.

[2]http://archive.eso.org

[3]ESO programme 113.26V6.001. PI: Iglesias.

Downloaded from https://academic.oup.com/mnras/article/550/4/stag1309/8732235 by guest on 31 July 2026

few km s^{-1} wide, hence cannot be photospheric in nature and must instead result from the absorption of stellar light by either interstellar or circumstellar gas (A. S. Hales et al. 2017). For later-type stars, the photospheric lines are intrinsically narrower, making it more difficult to distinguish them from non-photospheric components. The Ca II K line in particular is a well-known tracer of circumstellar (and interstellar) gas and is widely used to identify gas-bearing debris discs. This line is most sensitive to the transit of gaseous clouds, such as those produced by exocomets (F. Kiefer et al. 2014). In contrast, the Ca II H line absorption is usually half as strong as the Ca II K line (D. Iglesias et al. 2018), hence often undetectable in low signal-to-noise spectra (R. Bendahan-West et al. 2025). The Na I doublet is efficiently photoionized in the stellar UV radiation field, which is stronger than that of the ISM. Thus, there is often very little neutral sodium present in the circumstellar disc compared to ionized calcium (Ca II) (S. Redfield & J. L. Linsky 2002). While the Na I doublet is therefore a useful tracer of ISM gas, where a weaker radiation field allows it to remain in its neutral state, it is expected to be much less abundant inside a debris disc (but can still be detectable, e.g. like in β Pic, G. Olofsson, R. Liseau & A. Brandeker 2001).

Many of our targets had multiple observational epochs available, either from archival data or our UVES observations (see Table B1 for details). To ensure consistent continuum levels across the different epochs, we normalized each spectrum by rescaling the flux data within a radial velocity window of ±100 km s^{-1} centred on a specific spectral line, such that the maximum flux value was set to 1. Where multiple epochs were available, we combined the normalized spectra by computing the median flux at each wavelength point, improving the signal-to-noise ratio and isolating features that were consistently present across most observed epochs.

For most targets, we modelled the photospheric absorption using a polynomial (spline) fit, with the order of the polynomial selected interactively for each target to best reproduce the shape of the photospheric absorption profile. This method provides a good approximation of the stellar spectrum, particularly in cases where the narrow absorption features superimposed on top of it are stable across the observations. However, one object in our sample (discussed in Section 4.2.2), showed significant variability in its narrow absorption features. This made it difficult to accurately identify the photospheric absorption, making the spline fit unreliable for that object. To account for this, we fitted this single target's spectra using a Kurucz model (F. Castelli & R. L. Kurucz 2003), which is a synthetic stellar atmosphere model. While this model is generally more accurate, it is also significantly more complex and time-consuming to produce, making it impractical for most targets unless necessary. Since other objects in our sample do not exhibit significant variability or complexity, a spline fit was sufficient to model their stellar photospheres. The photosphere fits for the individual systems in which circumstellar gas is discussed in detail can be found in Appendix C (in Figures C1 and C2).

In both cases (spline and Kurucz model fit), the spectra were then divided by this fit to obtain continuum-subtracted spectra, isolating the narrow absorption features. For absorption lines showing a radial velocity shift in a cyclic manner over multiple epochs, we investigated the possibility of that object being a binary system. For this, we inspected the spectra for signs of line-doubling or cyclic variability, and searched the literature and relevant catalogues, e.g. SIMBAD (M. Wenger et al. 2000), VizieR (F. Ochsenbein, P. Bauer & J. Marcout 2000), for existing binarity classifications.

3.2 Characterizing the origin of narrow absorption features

We characterized the narrow absorption features detected in the Ca II K& H and Na I D1 & D2 lines by fitting them with Gaussian profiles, using either single or multiple components to model the continuum-subtracted spectra. The root-mean-square (RMS, σ) of the continuum was used to estimate the noise level, and only features with depths exceeding 3σ were considered detections. For each detected feature, we measured the radial velocity and intensity (depth) from its Gaussian fit. After characterizing the narrow features, our aim was to determine whether they were of interstellar or circumstellar origin. To do this, we followed the methodology from D. Iglesias et al. (2018), which included multiple diagnostic methods: (i) comparison with known interstellar clouds along the line of sight; (ii) comparison with narrow absorption features in spectra of nearby stars; (iii) comparison with the stellar radial velocity, since stable gas in Keplerian rotation should approximately match this velocity; and (iv) searching for variability across different epochs, which can indicate transient circumstellar gas.

To assess whether any of the detected narrow absorption features could be attributed to interstellar clouds, we used the S. Redfield & J. L. Linsky (2008) database[4], which catalogues 15 local interstellar clouds within 15 pc of the Sun and provides their predicted radial velocities. For each target, we used it to identify clouds lying directly along the line of sight or passing within 20° of it. For example, we found that TYC 6822-283-1 has a sight line transverse to the G cloud (-28.39 $\pm$ 1.13 km s^{-1}) and passes within 20° of the Gem and Aql clouds (-29.78 ± 1.07 km s^{-1} and -42.27 ± 1.17 km s^{-1}, respectively). However, because this database only covers the local ISM, it is incomplete for our most distant sources (up to $\sim$300 pc). We therefore also searched for interstellar contamination in the spectra of comparison stars located in similar sky directions.

The spectra of comparison stars were obtained from the ESO archive and our own observations (see Section 2.2 for details). We processed their spectra in the same manner as in our target sample, and calculated the angular separations between objects using TopCat (M. B. Taylor 2005). For each of our targets, we plotted only the residual flux as a function of radial velocity and directly compared it with the residual spectra of the nearby comparison stars. If a narrow absorption feature appeared at the same radial velocity (within uncertainties) in multiple neighbouring stars, we classified it as likely interstellar in origin.

To further investigate the nature of each detected gas absorption feature, we compared their measured radial velocity with the stellar radial velocities reported by D. P. Iglesias et al. (2023a), derived from X-shooter data. Gas rotating in a circumstellar disc is expected to match that velocity, and significant deviations can suggest an interstellar origin instead. For the three objects showing possible evidence of circumstellar gas, we calculated more precise stellar radial velocities using our higher resolution UVES spectra to improve the accuracy of this comparison. Infall- and outflow-driven absorption, commonly observed in earlier evolutionary stages (Class 0/1, C. J. Lada 1987), is not expected in our

[4] http://lism.wesleyan.edu/LISMdynamics.html

Downloaded from https://academic.oup.com/mnras/article/550/4/stag1309/8732235 by guest on 31 July 2026

Table 1. Parameters of objects discussed in this paper as having potential circumstellar gas, based on D. P. Iglesias et al. (2023a). Full list of objects from the D. P. Iglesias et al. (2023a) sample used in this study can be found in Table A1. TYC 6822-283-1 is marked with ^{i} as the origin of detected gas is inconclusive.

Name	Mass ($M_\odot$)	Luminosity ($L_\odot$)	SpT	Temperature (K)	Distance (pc)	Age (Myr)	F/F_{star} at 12 μm
HIP 30414	$2.87^{+0.67}_{-0.41}$	60.0 ± 20.0	A9/F0IV	7500 ± 500	190.39	$2.10^{+1.20}_{-1.00}$	$7.86^{+0.11}_{-2.27}$
TYC 7879-1373-1	$2.66^{+0.10}_{-0.23}$	60.0 ± 10.0	A0V	$10\,500 \pm 500$	225.64	$3.30^{+1.00}_{-0.30}$	$1.54^{+0.13}_{-0.11}$
TYC 6822-283-1^i	$2.50^{+0.18}_{-0.24}$	50.0 ± 10.0	A0V	$10\,700 \pm 700$	187.69	$4.00^{+2.00}_{-1.00}$	$6.21^{+0.55}_{-0.52}$

targets, which are more evolved and beyond that phase. Any gas detected in our targets will likely be rotating around the star and therefore have a projected radial velocity close to that of the star. However, transient phenomena such as accretion, disc winds, or exocomets may produce absorption offset from the stellar velocity, which we take into consideration when analysing individual systems.

Following the approach of D. Iglesias et al. (2018); D. P. Iglesias, O. Panić & I. Rebollido (2023b), we calculated the apparent column densities of narrow absorption features for the objects of interest using the methodology described by W. B. Somerville (1988). Oscillator strength values (f) were taken from D. C. Morton (1991), and equivalent width (EW) values were derived from our Gaussian profile fits. We also calculated the apparent column density ratios (Ca II / Na I, where the Ca II and Na I column densities correspond to the sums of K & H and D1 & D2 lines, respectively, see Table 2), which can serve as a diagnostic tool for assessing the origin of the absorption features. Ratios $\lesssim 1$ are typically associated with ISM gas, suggesting interstellar origin – although they do not fully exclude circumstellar nature (D. Iglesias et al. 2018).

4 RESULTS

4.1 Spectral analysis of gas features

Our spectral analysis is aimed at identifying new young debris disc systems that exhibit gas detectable through circumstellar absorption. We examined the Ca II K & H, and Na I D1 & D2 lines in the spectra of all 130 targets described in Section 2.1. Although most discs in this sample show low fractional IR excesses, their young ages make the primordial gas origin possible, although secondary origin cannot be ruled out.

To determine whether each feature originated from circumstellar or interstellar gas, we implemented methods described in Section 3.2. Reliable comparison between nearby stars required both similar distances and small angular separations, which are not always possible. Hence, where available, we used multiple comparison stars, since when multiple objects showed absorption at the same velocity, the likelihood of interstellar absorption increased significantly. Features that did not have such matches, remained stable over time, and were at the stellar radial velocity were considered likely circumstellar (F. Kiefer et al. 2014).

Across the sample, two stars showed absorption features consistent with circumstellar gas: HIP 30414 and TYC 7879-1373-1. In the case of TYC 6822-283-1, the origin is inconclusive. The parameters of these three systems are shown in Table 1. HIP 61782 (also known as HD 110058), which is also part of our sample, was previously confirmed to host circumstellar gas (A. S. Hales et al. 2017; D. Iglesias et al. 2018; I. Rebollido et al. 2018), hence we do not discuss it in detail here. Nevertheless, it is included in our sample for completeness, as our goal was to present the most comprehensive sample to date of all young intermediate-mass stars with 12 μm excess emission below protoplanetary disc level (D. P. Iglesias et al. 2023a).

We summarize the apparent column densities and EW of the detected narrow absorption features for the three objects showing possible circumstellar gas in Table 2. Following D. Iglesias et al. (2018), the Ca II / Na I apparent column density ratio can provide additional constraints on the nature of the gas, with values $\lesssim 1$ commonly associated with interstellar absorption, as the ISM typically contains more neutral sodium relative to ionized calcium due to its weaker radiation field compared to the circumstellar environment (S. Redfield & J. L. Linsky 2002). However, ratios above 1 are not a definitive indication of circumstellar nature, as some interstellar clouds can also produce high Ca II / Na I values, and hence this ratio cannot be used as a sole diagnostic. The features we classified as interstellar using other methods (detailed in Section 3.2) generally have Ca II / Na I < 1, while features we identified as likely circumstellar have larger Ca II / Na I ratios. This behaviour is consistent with previous studies, but can only be used as a tool in combination with other diagnostic methods.

4.2 Gas of possible circumstellar origin

4.2.1 TYC 7879-1373-1

The spectrum of TYC 7879-1373-1 (Fig. 2, left) shows three narrow absorption features in the Ca II K line at $-11.33\,\mathrm{km\,s^{-1}}$ (7.4σ), -4.02 $\mathrm{km\,s^{-1}}$ (42.6σ), and 2.04 $\mathrm{km\,s^{-1}}$ (27.9σ). We compared it with spectra of four nearby stars – two from our sample and two from the ESO archive. The first absorption feature does not match any known interstellar clouds or absorption features in the spectra of nearby stars, but matches the stellar radial velocity of $-10.68 \pm 1.64\,\mathrm{km\,s^{-1}}$. This feature is absent in the Na I D1 and D2 lines, but is prominent in both Ca II K & H lines. This first narrow gas absorption feature has an apparent column density ratio of (Ca II / Na I) of 3.67 (Table 2), which strengthens its circumstellar nature. We find that TYC 7879-1373-1 shows no evidence of ongoing accretion.

4.2.2 HIP 30414 (HD 44892): variable circumstellar gas?

Most of the variable features we identified in our sample were found in spectroscopic binary systems, where changes between each epoch result from the orbital motion between the component stars. However, one object in our sample, HIP 30414 (also known as HD 44892), exhibits variability that cannot be attributed to binarity. As shown in Fig. 3, the spectra of HIP 30414 change between the two observed epochs. To distinguish stellar absorption from narrow, possibly circumstellar features, we fitted the spectra using Kurucz photospheric models (spectra created

Downloaded from https://academic.oup.com/mnras/article/550/4/stag1309/8732235 by guest on 31 July 2026

Table 2. Parameters of absorption features found in spectra of each object, stated for each line, including the feature's radial velocity, apparent column density, and EW. The last column is the apparent column ratio of Ca II to Na I. Parameters of features of suspected circumstellar origin are shaded. TYC 6822-283-1 is marked with ^{i} as the origin of detected gas is inconclusive. ^{UL} denotes an upper limit where no feature is detected. Parameters of HIP 30414 are presented for both of its observed epochs to show variability between them. *Uncertainties are of order 2–4 per cent for Ca II and 1–2 per cent for Na I.

	Ca II K*			Ca II H*			Na I D1*			Na I D2*			
Name	RadV (km s^{-1})	$\log_{10}$N (cm^{-2})	EW (mÅ)	RadV (km s^{-1})	$\log_{10}$N (cm^{-2})	EW (mÅ)	RadV (km s^{-1})	$\log_{10}$N (cm^{-2})	EW (mÅ)	RadV (km s^{-1})	$\log_{10}$N (cm^{-2})	EW (mÅ)	$\frac{\mathrm{N[CaII]}}{\mathrm{N[NaI]}}$
HIP 30414 epoch 1	*Variable*	12.43	232.38	*Variable*	12.53	148.26	*Variable*	12.14	133.73	*Variable*	11.89	150.10	2.85
	22.47	11.73	47.11	21.56	11.80	27.40	22.66	12.14	132.75	22.62	11.88	146.57	0.55
HIP 30414 epoch 2	*Variable*	12.42	229.62	*Variable*	12.50	138.86	*Variable*	12.14	133.54	*Variable*	11.88	147.94	2.74
	23.09	11.75	48.68	22.53	11.83	29.92	22.69	12.14	132.36	22.68	11.88	145.58	0.59
TYC 7879-1373-1	−11.46	10.44	2.36	−13.30	10.71	2.25	–	10.21^{UL}	1.57^{UL}	–	9.71^{UL}	0.98^{UL}	3.67
	−3.94	11.46	25.06	−4.15	11.55	15.49	−4.41	11.97	90.66	−4.59	11.68	92.54	0.45
	1.43	11.42	12.86	1.74	11.58	7.41	1.25	12.03	103.64	1.06	11.78	117.68	0.38
TYC 6822-283-1^{i}	−16.01	11.27	16.14	−16.92	11.50	13.77	−16.63	10.56	3.54	−15.82	10.96	17.49	3.98
	–	10.46^{UL}	2.49^{UL}	–	10.80^{UL}	2.78^{UL}	−11.66	11.06	11.21	−11.33	11.15	27.11	0.35
	−5.53	10.82	5.77	−5.36	11.14	6.09	−5.47	11.87	71.39	−5.39	11.65	87.43	0.17
	0.31	11.61	35.30	0.22	11.71	22.64	1.02	11.33	20.85	1.20	11.33	41.45	2.14
	7.16	11.45	24.54	6.74	11.57	16.15	7.42	10.92	8.06	7.55	10.88	14.54	4.07
	12.29	10.29	1.71	10.97	10.82	2.91	–	10.21^{UL}	1.57^{UL}	–	9.31^{UL}	0.39^{UL}	4.68

using VidmaPy[5], models from F. Castelli & R. L. Kurucz (2003, see Fig. C1), which are more accurate than simpler polynomial fits (D. Iglesias et al. 2018).

After removing the photospheric contribution, the residual flux of both epochs shows a stable feature, present in all four of the analysed lines, at a radial velocity of 22.47 km s^{-1} (35.7σ) in the Ca II K line. Although it matches the stellar radial velocity of 20.88 ± 1.85 km s^{-1}, this feature is also well matched by interstellar clouds and by absorption features seen in the spectra of nearby comparison stars. Hence, we cannot rule out its interstellar nature.

To quantify the variability of the remaining absorption, we measured EWs independently for each epoch in the analysed Ca II and Na I lines. EWs were calculated over a radial velocity range from −65 km s^{-1} to 50 km s^{-1}, excluding the stable interstellar feature. The rms noise level (σ) was estimated using continuum regions outside this range. For the Ca II K line, we found the EWs for epochs 1 and 2 to be 232.38 mÅ (37σ) and 229.62 mÅ (51σ), respectively. In the Ca II H line, these are 148.26 mÅ (45σ) and 138.86 mÅ (55σ), for the same epochs. The full results are summarized in Table 2.

Since the EWs between the two epochs are very similar, we chose to showcase the variability by fitting Gaussian curves to Ca II K & H lines. As shown in Fig. 4, both the positions of the Gaussian peaks and their intensity needed to fit the variable residual absorption change between the two epochs. In the second epoch, significant absorption begins at ∼−35 km s^{-1}, while in the 1st epoch it extends to ∼-55 km s^{-1}. The position of the main component also shifts between the two epochs from −2.11 km s^{-1} to 10.78 km s^{-1} in Ca II K and −2.41 km s^{-1} to 10.85 km s^{-1} in Ca II H. The depth of this component changes by 13.4 per cent and 12.2 per cent between the two epochs in Ca II K & H, respectively.

For the variable features of HIP 30414, the apparent column density (Ca II / Na I) ratios (Table 2) are quite high (∼2.8) whereas the ratios for the stable feature at ∼22 km s^{-1} are much lower (∼0.6). While these ratios alone are not sufficient to determine the nature of gas, their significant difference supports an interstellar origin for the stable component and a circumstellar nature for the variable absorption.

HIP 30414 is also the only object in our sample exhibiting variability in the H$_\alpha$ line (see Fig. 5). The residual H$_\alpha$ spectrum, obtained by normalizing the observed flux by the fitted Kurucz model, is a composite of emission and absorption components. The relative strength of absorption and emission differs between the two epochs; in epoch 2, the central absorption dominates over emission and extends below the continuum level. Using methods described in J. R. Fairlamb et al. (2017), we estimate the mass accretion rates in the two epochs as $\log \dot{M}_{\rm acc} = -7.64^{+0.11}_{-0.07}$ M$_\odot$ yr^{-1} and $\log \dot{M}_{acc} = -7.69^{+0.11}_{-0.07}$ M$_\odot$ yr^{-1}.

4.3 Inconclusive gas origin

4.3.1 TYC 6822-283-1

The spectrum of TYC 6822-283-1 has multiple absorption features in the Ca II K line (Fig. 2, right), all of which are above the noise threshold (3σ) and were best fitted with a combination of five Gaussian functions. The last two peaks in Ca II K, at 7.16 km s^{-1} (36.5σ) and 12.29 km s^{-1} (10.7σ), do not match with the spectra of nearby stars or interstellar clouds, nor do they match the stellar radial velocity. Therefore, with the current observations, we do not have enough information to classify the origin of these features. Their apparent column density ratio (Table 2) are high (> 4), yet this diagnostic alone, as discussed in Section 4.1, is not enough to conclusively determine the nature of the gas. Additionally, we find no evidence of ongoing accretion in the spectrum of TYC 6822-283-1.

4.4 Gas of interstellar origin

The majority of the narrow absorption features we detected in our sample are consistent with an interstellar gas origin. These

[5]https://github.com/RozanskiT/vidmapy

Downloaded from https://academic.oup.com/mnras/article/550/4/stag1309/8732235 by guest on 31 July 2026

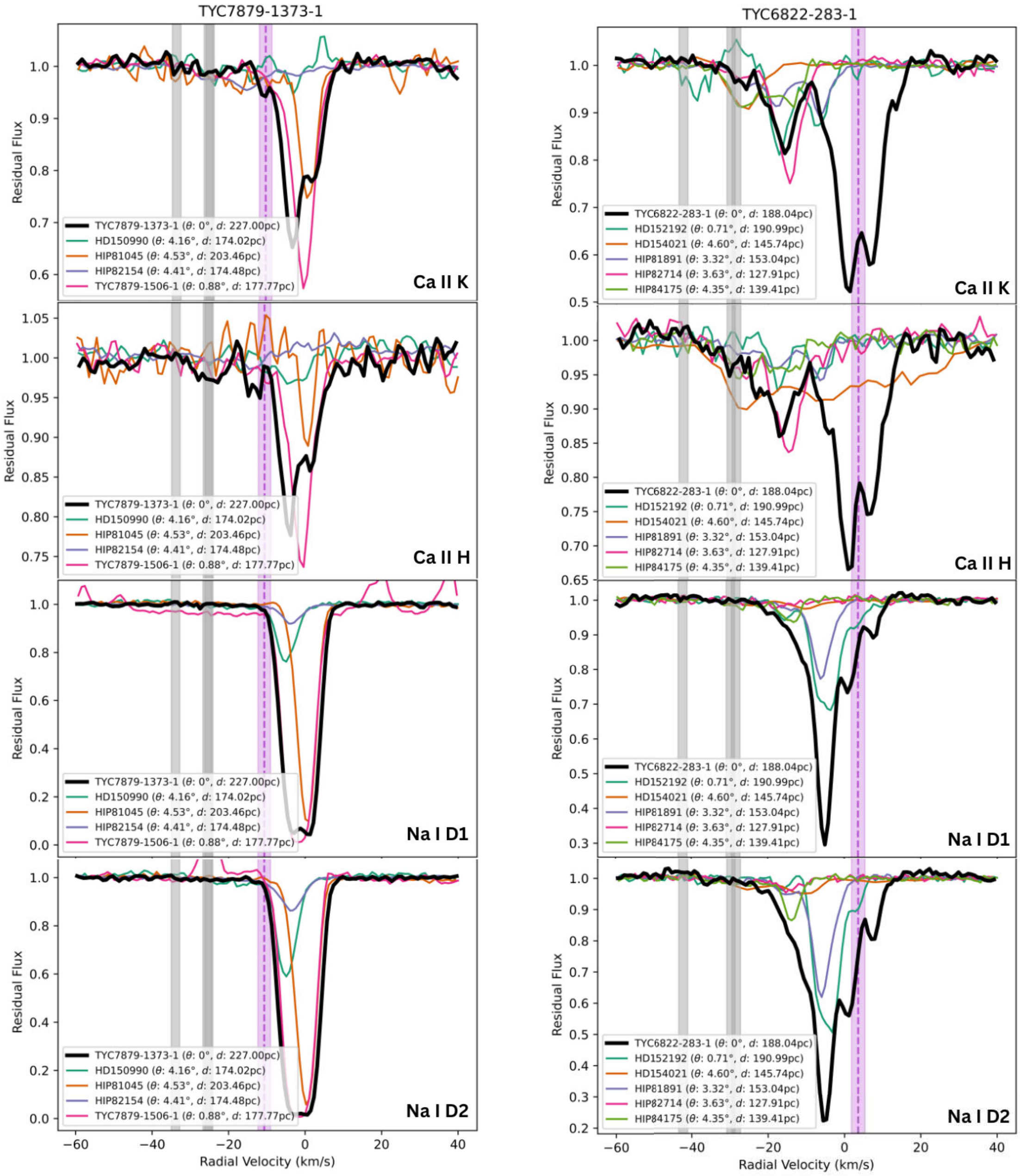

Figure 2. **Left:** Residual flux versus radial velocity (km s^{-1}) showing three isolated narrow absorption features in the Ca II K & H and Na I D1 & D2 lines of TYC 7879-1373-1 (in black), which, in Ca II K, are -11.33 km s^{-1} (7.4σ), -4.02 km s^{-1} (42.6σ), and 2.04 km s^{-1} (27.9σ), respectively. The known velocities of clouds in the line of sight are plotted in grey. Comparison stars with their narrow absorption features are plotted in various colours, with their distances and angular separations from TYC 7879-1373-1 stated. The pink region corresponds to the radial velocity of TYC 7879-1373-1, -10.68 ± 1.64 km s^{-1}. **Right:** Same but for TYC 6822-283-1. Radial velocity of TYC 6822-283-1 is 3.60 ± 1.77 km s^{-1}. The five narrow absorption features detected in Ca II K line are -16.01 km s^{-1} (12.9σ), -5.53 km s^{-1} (10.2σ), 0.31 km s^{-1} (37.0σ), 7.16 km s^{-1} (36.5σ), and 12.29 km s^{-1} (10.7σ).

features either matched the radial velocities of known interstellar clouds, features found in the spectra of nearby stars, or were detected at velocities not consistent with the stellar radial velocities reported by D. P. Iglesias et al. (2023a). Based on these criteria, we classify 111 targets as having absorption features likely interstellar in origin.

In some cases, the depths of absorption-like features were close to our 3σ detection threshold; hence, we examined their presence across individual epochs. If a feature persisted at the same radial velocity for all epochs and exceeded 3σ, we considered it to be a detection; if it was not consistent, we deemed it unreliable and thought of it as noise. Across the full sample, we found 15 targets that showed no reliable narrow absorption features.

HIP 48613 is an example of a target we ultimately classified as having interstellar gas absorption. The system exhibits a narrow absorption feature close to the stellar radial velocity (feature: 16.46 km s^{-1}, stellar: 15 ± 8 km s^{-1}) that did not correspond to

Downloaded from https://academic.oup.com/mnras/article/550/4/stag1309/8732235 by guest on 31 July 2026

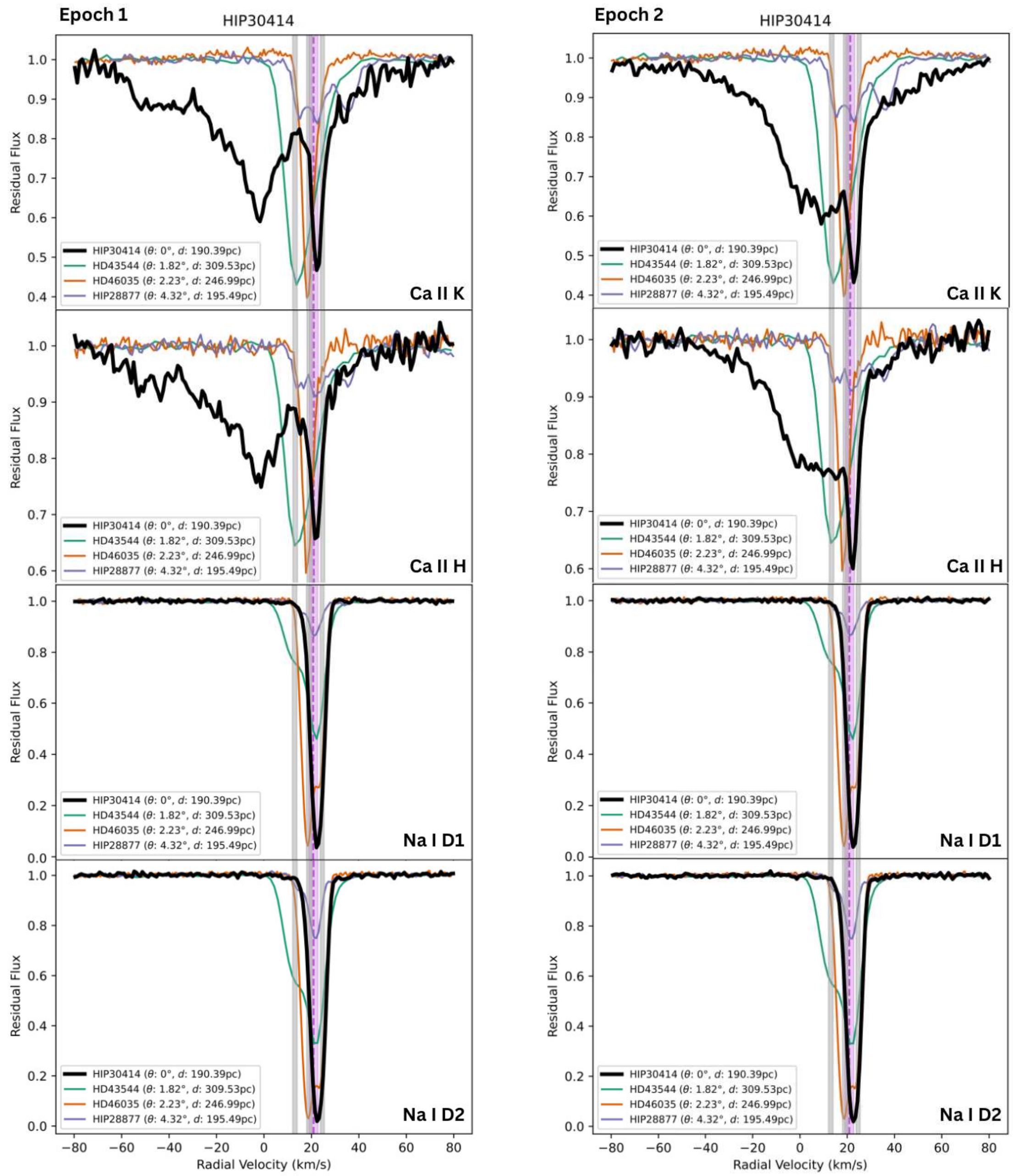

Figure 3. Left: Residual flux versus radial velocity (km s^{-1}) for epoch 1, showing variable isolated narrow absorption features in the Ca II K & H and Na I D1 & D2 lines of HIP 30414 (in black). The known velocities of clouds in the line of sight are plotted in grey. Comparison stars with their narrow absorption features are plotted in various colours, with their distances and angular separations from HIP 30414 stated. The pink region corresponds to the radial velocity of HIP 30414, 20.88 ± 1.85 km s^{-1}. **Right:** Same but for epoch 2 of HIP 30414.

any known interstellar clouds and was not fully reproduced in the spectra of comparison stars. However, HIP 48613 is a spectroscopic binary, and while its stellar spectrum varied between the observed epochs due to orbital motion, three narrow absorption features remained constant across epochs. Such behaviour is unexpected for absorption arising in a circumstellar disc around either individual star, as these features would be expected to shift with the host star. Although a circumbinary disc could in principle produce such stationary absorption, these features are also strongly present in Na I D1 & D2 lines and matched by comparison stars in sodium absorption. Given that Na I is a tracer of interstellar gas (D. Iglesias et al. 2018), this strongly supports an interstellar origin for the absorption features in HIP 48613.

5 DISCUSSION

5.1 Identification of circumstellar gas

We searched for circumstellar gas by identifying narrow absorption lines in stellar spectra, which indicate the presence of gas along the line of sight to the star. Detecting such features is inherently biased towards systems viewed close to edge-on, where

Downloaded from https://academic.oup.com/mnras/article/550/4/stag1309/8732235 by guest on 31 July 2026

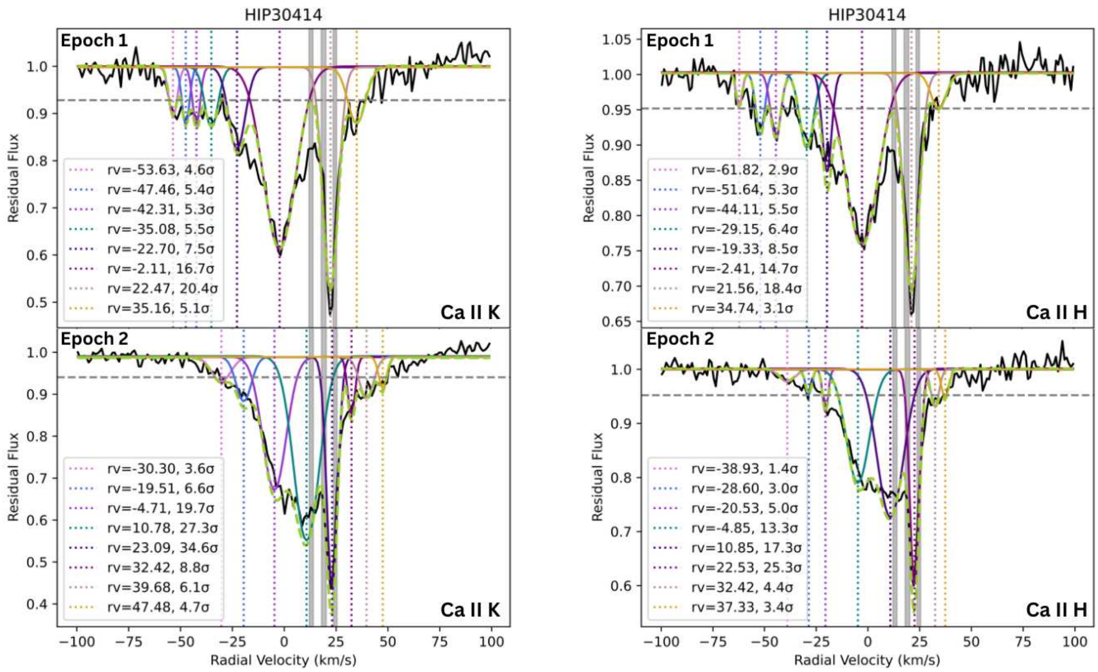

Figure 4. Changes in residual flux in the Ca II K (left) and Ca II H (right) lines of HIP 30414 across two epochs. The residual flux in each epoch is fitted with Gaussian curves, the positions and intensities of which vary between epochs 1 and 2. The composite Gaussian fit is shown as a green dashed line, while the residual flux is plotted in black. The positions and intensities of individual Gaussian components are marked accordingly.

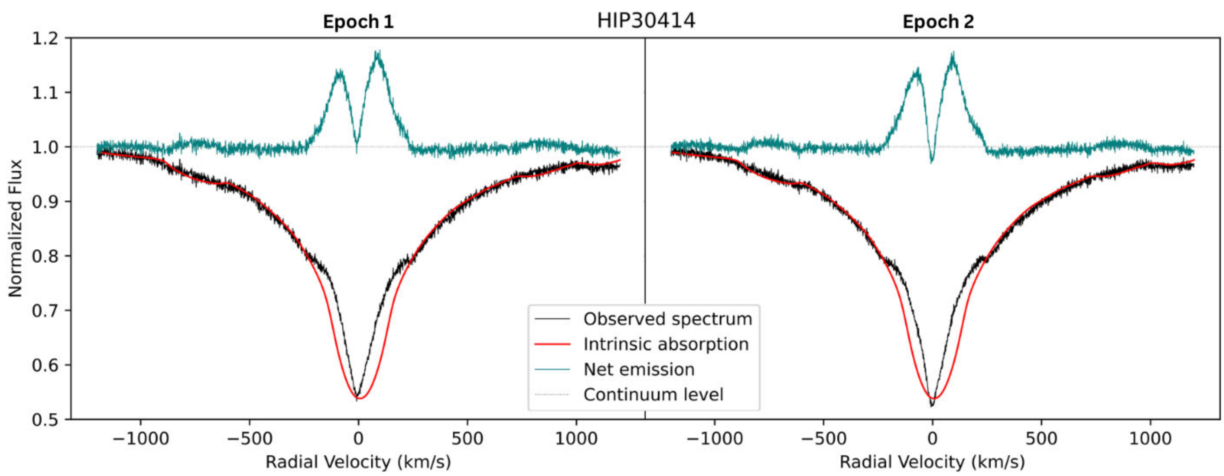

Figure 5. Changes in the H_α features across the two observed epochs of HIP 30414. Left panel shows epoch 1, and the right panel shows epoch 2. The observed flux is plotted in black, while the Kurucz model used for this fit is shown in red (parameters: temperature 7000 K, log(g) 3.6, [Fe/H] 0, and $v\sin(i)$ 140 km s^{-1}). The residual (net) emission, shown in teal, contains both emission and absorption features. In epoch 2, the central absorption extends below the continuum level.

the observer's line of sight passes through the circumstellar gas disc (A. S. Hales et al. 2017; A. M. Hughes et al. 2018). The two gas-bearing debris disc systems we identified within our sample, TYC 7879-1373-1 and HIP 30414, are very young (< 5 Myr), and are classified as pre-MS stars – likely caught in the transition from protoplanetary to debris discs, with gas that may still be primordial (R. Nakatani et al. 2021). Their masses (2.66 and 2.87 M$_\odot$, respectively) place them in the intermediate mass regime, where most circumstellar gas detections have been reported (M. C. Wyatt et al. 2015).

Fig.6 presents the ages and 12 µm fractional excesses of the 135 targets from D. P. Iglesias et al. (2023a), including the five protoplanetary discs (PPDs) we did not analyse. HIP 30414 occupies the region between protoplanetary and debris discs, while TYC 7879-1373-1 is placed firmly in the debris category by the level of 12 µm fractional excess. TYC 6822-283-1, for which the origin of gas remains inconclusive, and HIP 61782, in which gas has been detected by multiple past studies (A. S. Hales et al. 2017; D. Iglesias et al. 2018; I. Rebollido et al. 2018), are also shown for context. In the following sections, we examine in detail the gas

Downloaded from https://academic.oup.com/mnras/article/550/4/stag1309/8732235 by guest on 31 July 2026

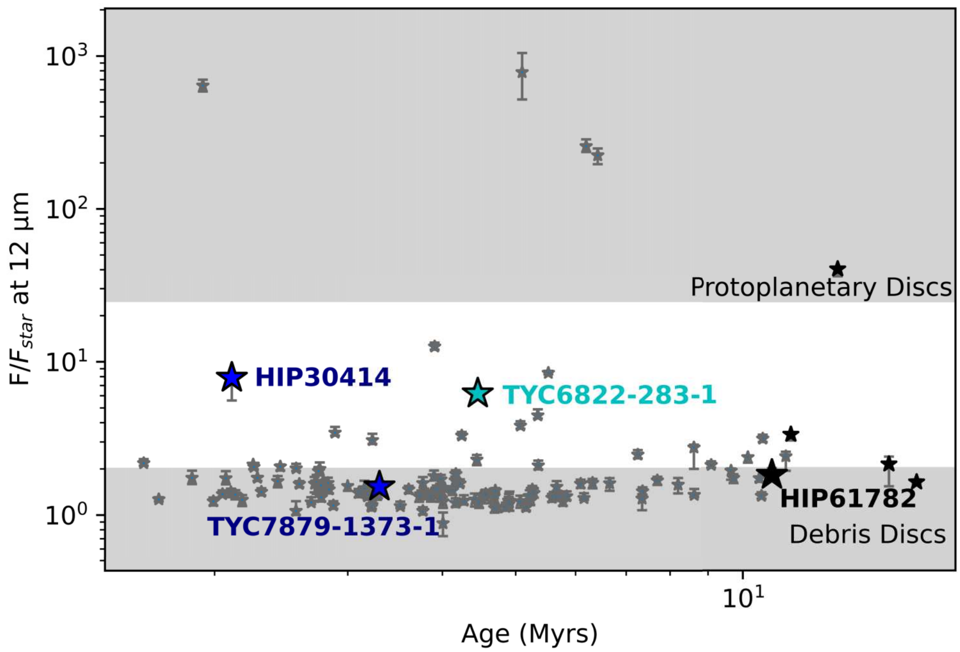

Figure 6. Excess emission at 12 μm versus age of 135 identified objects in D. P. Iglesias et al. (2023a), plotted with excess uncertainties. Debris and protoplanetary disc regions are shaded. The identified gas-bearing discs are marked, including HIP 61782 not discussed in detail here. The discs caught between protoplanetary and debris disc regimes are: HIP 30414 and TYC 7879-1373-1, marked in blue. TYC 6822-283-1, for which the origin is inconclusive, is also marked. Stars marked in black indicate the objects that may already be on the MS.

absorption features detected towards these systems (excluding HIP 61782). Where sufficient data is available, we compare our results with previous studies to provide additional insight and place our findings in a broader context.

5.2 Debris discs with circumstellar gas

5.2.1 TYC 7879-1373-1

D. P. Iglesias et al. (2023a) classify TYC 7879-1373-1 as a debris disc; however, there are no other mentions of this object in the literature relevant to our study. It exhibits a narrow absorption feature suspected to be of circumstellar origin, as it closely matches the stellar radial velocity. This feature does not correspond to absorption in nearby comparison stars or known interstellar clouds and is also absent from Na I lines, supporting its circumstellar nature.

Given its young age, TYC 7879-1373-1 is a strong candidate for hosting a gas-bearing debris disc and an important system for understanding the transition from protoplanetary to debris discs. Further observations, such as gas emission studies, are needed to characterize the gas disc in more detail. Nonetheless, based on the available data, we consider this detection to originate from circumstellar gas.

5.2.2 HIP 30414 (HD 44892): variable circumstellar gas

Based on the H_α line, we found that the pre-MS star HIP 30414 is undergoing active accretion, which makes the inner disc a strong candidate for retaining primordial circumstellar gas. Evidence for a dusty circumstellar disc was first suggested by B. M. Patten & L. A. Willson (1991), who reported the presence of 12 and 25 μm excesses detected with IRAS. D. Ishihara et al. (2017) also identified it as a debris disc candidate based on the level of IR excess emission found at 18 μm, while D. P. Iglesias et al. (2023a) first reported it as a'hybrid disc candidate' due to its relatively high 12 μm excess.

The residual spectra of HIP 30414 show variability that is absent from the spectra of nearby stars in the corresponding radial velocity range. Similarly, no known interstellar clouds are present in this velocity range. The stable feature at $\sim$22 km s^{-1} is well matched by the best available comparison star, HIP 28877, in all lines, including sodium, confirming its interstellar origin. However, the variable absorption component, which is seen in both Ca II lines, is not detected in Na I lines and does not correspond to any known interstellar clouds. This strongly suggests that the variable feature arises from transient circumstellar gas, like exocomets (like in β Pic W. R. F. Dent et al. 2014), a wind disc (like in NO Lup J. B. Lovell et al. 2021b), or accretion.

The correlation in variability in the Ca II lines and the H_α line indicates that the gas is hot and located close to the star, and likely primordial rather than secondary in origin, as secondary gas would be unlikely to sustain the high accretion rate we derived (see Section 4.2.2). Given that HIP 30414 is actively accreting, the variability we observed is most likely associated with the ongoing accretion rather than exocomets or winds. Furthermore, as the gas absorption in the H_α line overcomes much of the gas emission, the system is likely seen edge-on.

Further supporting the presence of circumstellar gas in HIP 30414 is the recent discovery of ^{12}CO ($J = 2 - 1$) and continuum emission with ALMA in this debris disc in K. M. Szewczyk et al. (2025). The reported CO gas mass in this disc is between 10^{-4} M$_\oplus$ and 10^{-2} M$_\oplus$. This detection, combined with the evidence of ongoing gas accretion, suggests that HIP 30414 may be in the rare transitional phase between protoplanetary and debris disc stages.

Downloaded from https://academic.oup.com/mnras/article/550/4/stag1309/8732235 by guest on 31 July 2026

5.3 Inconclusive gas origin

5.3.1 TYC 6822-283-1

TYC 6822-283-1 was first reported as a'hybrid disc candidate' by D. P. Iglesias et al. (2023a), who also first identified its IR excess levels in the *WISE W*1–*W*4 bands, between protoplanetary and debris disc levels. We found that the spectrum of TYC 6822-283-1 exhibits two pronounced absorptions with no clear origin (Fig. 2, right). These features do not correspond to known interstellar clouds or nearby stars, nor do they precisely match the stellar radial velocity. This object is located in a region where multiple interstellar clouds are present, complicating the classification. While it could originate from circumstellar gas, an interstellar origin cannot be ruled out.

On the age vs 12 μm fractional excess plot (Fig. 6), TYC 6822-283-1 has a relatively high level of IR excess, suggesting the presence of substantial dust in the disc. Its estimated age of 4 Myr (D. P. Iglesias et al. 2023a) classifies it as a pre-MS star, increasing the likelihood of retaining detectable primordial gas. We searched the literature and found no relevant studies that could provide insight into the origin of these features; hence, it remains inconclusive until we are able to collect further evidence.

6 CONCLUSIONS

We analysed the spectra of 130 pre-MS debris discs and 'hybrid disc candidates' from D. P. Iglesias et al. (2023a), searching for narrow absorption features in Ca II K & H and Na I D1 & D2 lines that could indicate the presence of circumstellar gas. Absorption spectroscopy is most effective for identifying gas along the line of sight, favouring systems where the disc is viewed edge-on. Because of this observational bias, the likelihood of interstellar origin of the gas absorption lines is high; hence, we employed several diagnostic methods to determine the nature of the features. This included comparison to nearby stars, searching for variability between observed epochs, calculating line ratios, and others (see Section 3.2 for details), to distinguish between circumstellar and interstellar nature.

Through this process, we identified two new systems with likely circumstellar gas: TYC 7879-1373-1, which is a new detection, and HIP 30414, in which CO gas emission was previously identified by K. M. Szewczyk et al. (2025). We also confirm the presence of a gas disc in HIP 61782, where circumstellar absorption was previously reported by A. S. Hales et al. (2017), D. Iglesias et al. (2018), and I. Rebollido et al. (2018), hence we do not discuss this system in detail. In addition, one system, TYC 6822-283-1, shows narrow absorption features for which the origin of gas remains inconclusive based on our diagnostic methods. Out of the remaining targets, 111 systems show features that are interstellar in origin, while 15 candidates exhibit no detectable narrow absorption features in the analysed lines. Our results are summarised in Table A1. Despite the small number of circumstellar detections, our results show that absorption spectroscopy is a time-effective screening tool when searching for gas-bearing discs within large target samples.

The two new systems with likely circumstellar gas are both pre-MS stars (< 5 Myr), with stellar masses of 2.66 $M_\odot$ (TYC 7879-1373-1) and 2.87 $M_\odot$ (HIP 30414), placing them in the intermediate mass regime where circumstellar gas is most commonly detected (M. C. Wyatt et al. 2015; A. M. Hughes et al. 2018). Their young ages suggest that the gas in them may still be of primordial origin (R. Nakatani et al. 2021; G. V. Smirnov-Pinchukov et al. 2022), although we cannot rule out the secondary origin. HIP 30414, in particular, shows evidence of ongoing active accretion based on the variability in Hα emission we have measured. This provides further evidence for the presence of primordial gas located close to the star. TYC 6822-283-1 is also a very young (4 Myr) intermediate mass star (2.50 $M_\odot$), however, until we are able to collect more data, we cannot rule out the possibility of the interstellar nature of the detected gas.

Assuming the typical vertical aspect ratio of debris discs as 0.07, taken as a median of values from the REASONS study (L. Matrà et al. 2025), a typical angle such a disc spawns is 4°. For a uniform distribution of sin(i) between 0 and 1, the probability of $90^\circ - 4^\circ \leq i \leq 90^\circ + 4^\circ$ (i.e. near edge-on disc) is ~7 per cent (corresponding to ~9 discs in our sample). Out of 130 systems, we detect likely circumstellar features in three discs, including HIP 61782 (which is confirmed to be a near edge-on disc in S. Hales et al. 2022). This corresponds to ~33 per cent of discs observed near edge-on, considering a uniform distribution of inclinations. While this suggests that around a third of edge-on debris discs in our sample may exhibit detectable gas absorption, the detection number is small and hence this estimate is highly uncertain and should not be considered as representative of the full debris disc population. Nevertheless, our full sample is not located in one place in the sky or limited to star-forming regions, reducing observational bias.

While the circumstellar origin of their features cannot be certain, additional studies can help determine their nature. Future observations can confirm the presence of gas-bearing discs in the identified systems. For TYC 7879-1373-1, ALMA observations targetting continuum and CO line emission could reveal the dust and gas morphology. HIP 30414 has already been observed as part of the ALMA programme 2022.1.01686.S (PI Panić), with ^{12}CO gas and dust emission detected in a Keplerian disc (K. M. Szewczyk et al. 2025). TYC 6822-283-1 was also scheduled for ALMA observations under the same programme; however, these were never completed. Continued multiwavelength studies, including high-resolution spectroscopy and interferometry, will be crucial to better understand the transition from protoplanetary to debris discs and how gas affects planetary systems' evolution.

ACKNOWLEDGEMENTS

KS acknowledges funding from the Bell Burnell Graduate Scholarship Fund (BB0023). DPI and OP acknowledge support from the Science and Technology Facilities Council via grant number ST/X001016/1.

This work has made use of data from the European Space Agency (ESA) mission *Gaia* (https://www.cosmos.esa.int/gaia), processed by the *Gaia* Data Processing and Analysis Consortium (DPAC, https://www.cosmos.esa.int/web/gaia/dpac/consortium). Funding for the DPAC has been provided by national institutions, in particular the institutions participating in the *Gaia* Multilateral Agreement.

Based on observations collected at the European Southern Observatory under ESO programmes: 112.262P.001, 110.23YZ.001, 113.26V6.001, 109.23K8.001, 092.C-0721(A), 073.D-0049(A), 085.A-9027(B), 098.C-0463(B), 0102.A-9008(A), 0103.C-0206(A), 096.A-9024(A), 194.C-0833(D), 099.D-0380(A), 087.C-0012(B), 075.D-0676(B), 095.A-9029(C), 078.D-0080(A), 092.A-9006(A), 076.D-0169(A), 0100.C-0090(B), 178.D-0361(B), 67.D-0133(A), 099.C-0491(A), 078.A-9059(A), 0101.D-0697(A), 098.C-0739(A),

Downloaded from https://academic.oup.com/mnras/article/550/4/stag1309/8732235 by guest on 31 July 2026

68.C-0548(A), 072.C-0488(E), 087.A-9013(A), 080.C-0712(A), 194.C-0833(H), 076.C-0279(A), 182.D-0356(B), 090.C-0421(A), 099.C-0637(A), 074.C-0135(A), 185.D-0056(E), 072.D-0021(B), 0106.A-9009(A), 085.D-0093(A), 099.A-9022(A), 0106.A-9006(A), 089.D-0129(A), 085.A-9027(A), 089.C-0006(A), 079.A-9009(A), 087.C-0012(A), 183.C-0972(A), 075.C-0637(A), 080.D-0194(A), 185.D-0056(B), 082.C-0446(B), 083.C-0676(A), 194.C-0833(B), 0102.D-0281(A), 097.A-9024(A), 085.A-9027(G), 097.A-9022(A), 0101.A-9016(A), 096.A-9039(A), 076.D-0018(A), 099.A-9009(A), 073.A-9008(A), 106.20Y7.002, 079.B-0856(A), 099.A-9029(A), 179.C-0197(D), 075.D-0760(A), 190.C-0027(A), 083.A-9014(B), 266.D-5655(A), 075.D-0324(A), 105.20L8.002, 081.C-0475(A), 079.A-9014(A), 079.D-0118(A), 077.C-0547(A), 073.C-0337(A), 075.D-0103(A), 087.C-0831(A), 0101.C-0232(C), 088.C-0353(A), 0103.C-0548(A), 097.C-0409(B), 185.D-0056(I), 185.D-0056(C), 091.C-0713(A), 67.D-0579(A), 079.C-0789(A), 0104.A-9010(A), 084.D-0067(A), 0100.C-0097(A), 0102.C-0338(A), 074.D-0008(B), 0104.A-9004(A), 184.C-0815(E), 094.C-0946(A), 082.C-0446(A), 081.C-2003(A), 179.C-0197(C), 0103.A-9009(A), 084.A-9011(B), 075.C-0479(A), 083.A-9013(A), 090.D-0358(A), 185.D-0056(A), 088.A-9029(A), 072.D-0021(A), 097.C-0090(A), 088.D-0026(D), 073.D-0641(A), 0103.A-9011(A), 0102.A-9010(A), 179.C-0197(A), 082.C-0831(A), 073.D-0724(A), 0100.A-9006(A), 077.D-0247(A), 0102.C-0584(A), 087.B-0600(G), 085.C-0019(A), 66.D-0457(A), 105.2045.001, 093.C-0658(A), 0102.C-0547(A), 0104.A-9003(A), 083.D-0034(A), 106.21R4.001, 60.A-9700(A), 077.C-0192(A), 097.C-0409(A), 075.C-0689(B), 097.D-0150(A), 0101.C-0232(A), 095.A-9032(A), 0100.C-0414(B), 71.B-0529(A), 0108.A-9006(A), 087.A-9029(A), 087.D-0950(B), 093.C-0409(A), 0101.A-9001(A), 184.C-0815(A), 0101.D-0415(A), 077.C-0575(A), 096.A-9027(A), 293.D-5036(A), 0101.D-0921(A), 098.C-0463(C), 089.D-0975(A), 184.C-0815(C), 083.C-0139(A), 098.A-9039(C) 380.C-0083(A) 077.C-0295(D), 093.D-0302(A), 096.A-9018(A), 074.D-0021(A), 076.C-0279(B), 079.D-0009(C), 077.C-0295(A), 0104.C-0418(C), 091.D-0221(A), 092.A-9002(A), 0101.A-9005(A), 072.D-0149(A), 077.C-0295(B), 105.2045.002, 087.D-0010(A), 0108.A-9029(A), 092.C-0173(A), 105.2055.001, 075.D-0597(A), 0102.C-0040(B), 096.C-0238(A), 094.A-9012(A), 082.D-0061(A), 69.C-0171(A), 076.C-0279(C), 077.D-0720(B), 184.C-0815(F), 075.C-0689(A), 380.C-0083(B), 165.N-0276(A), 60.A-9700(G), 082.B-0484(A), 0104.A-9001(A), 084.B-0029(A), 079.D-0567(A), 088.D-0026(D), 075.D-0145(A), 095.A-9029(C), 074.D-0240(A), 080.C-0032(B), 079.C-0170(A), 074.C-0102(A), 075.C-0234(A), 082.C-0308(A), 080.C-0032(A), 076.C-0073(A), 095.D-0717(A), 080.D-0191(A), 072.D-0196(A), 077.D-0478(A), and 0103.D-0119(A).

DATA AVAILABILITY

All data underlying this article are available in the ESO and GAIA archives. ESO data are found at http://archive.eso.org/cms.html. GAIA archive can be browsed at https://gea.esac.esa.int/archive.

REFERENCES

Abt H. A., Moyd K. I., 1973, ApJ, 182, 809
Backman D. E., Paresce F., 1993, in Levy E. H., Lunine J. I. eds, Protostars and Planets III. p. 1253
Bendahan-West R., Kennedy G. M., Brown D. J. A., Strøm P. A., 2025, MNRAS, 537, 229
Brennan A. et al., 2024, MNRAS, 531, 4482
Castelli F., Kurucz R. L., 2003, in Piskunov N., Weiss W. W., Gray D. F., eds, IAU Symp. Vol. 210, Modelling of Stellar Atmospheres. p. A20, preprint (astro-ph/0405087)
Cataldi G. et al., 2023, ApJ, 951, 111
Chen C. H., Jura M., 2003, ApJ, 582, 443
Dekker H., D'Odorico S., Kaufer A., Delabre B., Kotzlowski H., 2000, in Iye M., Moorwood A. F., eds, Proc. SPIE Conf. Ser. Vol. 4008, Optical and IR Telescope Instrumentation and Detectors. SPIE, Bellingham, p. 534
Dent W. R. F. et al., 2014, Science, 343, 1490
Fairlamb J. R., Oudmaijer R. D., Mendigutia I., Ilee J. D., van den Ancker M. E., 2017, MNRAS, 464, 4721
Freudling W., Romaniello M., Bramich D. M., Ballester P., Forchi V., García-Dabló C. E., Moehler S., Neeser M. J., 2013, A&A, 559, A96
Haisch Jr K. E., Lada E. A., Lada C. J., 2001, ApJ, 553, L153
Hales A. S., Barlow M. J., Crawford I. A., Casassus S., 2017, MNRAS, 466, 3582
Hales Antonioand Marino S. et al., 2022, ApJ, 940, 161
Heays A. N., Bosman A. D., van Dishoeck E. F., 2017, A&A, 602, A105
Hernández J. et al., 2007, ApJ, 662, 1067
Hobbs L. M., Vidal-Madjar A., Ferlet R., Albert C. E., Gry C., 1985, ApJ, 293, L29
Hughes A. M., Duchêne G., Matthews B. C., 2018, ARA&A, 56, 541
Iglesias D., 2020, Searching for gas in debris disks, PhD thesis, Universidad de Valparaíso, Valparaíso, Chile
Iglesias D. et al., 2018, MNRAS, 480, 488
Iglesias D. et al., 2025, Space Sci. Rev., 221, 122
Iglesias D. P. et al., 2019, MNRAS, 490, 5218
Iglesias D. P. et al., 2023a, MNRAS, 519, 3958
Iglesias D. P., Panić O., Rebollido I., 2023b, MNRAS, 526, 2500
Inutsuka S.-I., Aikawa Y., Muto T., Tomida K., Tamura M. eds, 2023, ASP Conference Series Vol. 543, Protostars and Planets VII. Astronomical Society of the Pacific, San Francisco, CA
Ishihara D., Takeuchi N., Kobayashi H., Nagayama T., Kaneda H., Inutsuka S.-i., Fujiwara H., Onaka T., 2017, A&A, 601, A72
Kaufer A., Stahl O., Tubbesing S., Nørregaard P., Avila G., Francois P., Pasquini L., Pizzella A., 1999, Messenger, 95, 8
Kausch W. et al., 2015, A&A, 576, A78
Kiefer F., Lecavelier des Etangs A., Augereau J. C., Vidal-Madjar A., Lagrange A. M., Beust H., 2014, A&A, 561, L10
Kóspál Á. et al., 2013, ApJ, 776, 77
Koubsky P., Horn J., Harmanec P., Hubert A. M., Hubert H., Floquet M., 1993, A&A, 277, 521
Kral Q., Wyatt M., Carswell R. F., Pringle J. E., Matrà L., Juhász A., 2016, MNRAS, 461, 845
Kral Q., Matrà L., Wyatt M. C., Kennedy G. M., 2017, MNRAS, 469, 521
Kral Q., Marino S., Wyatt M. C., Kama M., Matrá L., 2019, MNRAS, 489, 3670
Kral Q., Davoult J., Charnay B., 2020a, Nat. Astron., 4, 769
Kral Q., Matrà L., Kennedy G. M., Marino S., Wyatt M. C., 2020b, MNRAS, 497, 2811
Lada C. J., 1987, in Peimbert M., Jugaku J., eds, IAU Symposium Vol. 115, Star Forming Regions. Springer, Dordrecht, p. 1
Lagrange-Henri A. M., Ferlet R., Vidal-Madjar A., Beust H., Gry C., Lallement R., 1990, A&AS, 85, 1089
Lieman-Sifry J., Hughes A. M., Carpenter J. M., Gorti U., Hales A., Flaherty K. M., 2016, The Astrophysical Journal, 828, 25
Lovell J. B. et al., 2021a, MNRAS, 500, 4878
Lovell J. B. et al., 2021b, MNRAS, 502, L66
Marino S. et al., 2016, MNRAS, 460, 2933
Marino S. et al., 2017, MNRAS, 465, 2595
Marino S., Cataldi G., Jankovic M. R., Matrà L., Wyatt M. C., 2022, MNRAS, 515, 507
Matrà L. et al., 2017, ApJ, 842, 9
Matrà L., Öberg K. I., Wilner D. J., Olofsson J., Bayo A., 2019, AJ, 157, 117
Matrà L. et al., 2025, A&A, 693, A151
Mayor M. et al., 2003, Messenger, 114, 20
Miley J. M., Panić O., Wyatt M., Kennedy G. M., 2018, A&A, 615, L10

Downloaded from https://academic.oup.com/mnras/article/550/4/stag1309/8732235 by guest on 31 July 2026

Montgomery S. L., Welsh B. Y., 2012, PASP, 124, 1042
Moór A. et al., 2017, ApJ, 849, 123
Moór A. et al., 2019, ApJ, 884, 108
Moór A. et al., 2025, A&A, 703, A15
Morton D. C., 1991, ApJS, 77, 119
Nakatani R., Kobayashi H., Kuiper R., Nomura H., Aikawa Y., 2021, ApJ, 915, 90
Nakatani R., Turner N. J., Hasegawa Y., Cataldi G., Aikawa Y., Marino S., Kobayashi H., 2023, ApJ, 959, L28
Ochsenbein F., Bauer P., Marcout J., 2000, A&AS, 143, 23
Olofsson G., Liseau R., Brandeker A., 2001, ApJ, 563, L77
Patten B. M., Willson L. A., 1991, AJ, 102, 323
Péricaud J., Di Folco E., Dutrey A., Guilloteau S., Piétu V., 2017, A&A, 600, A62
Rebollido I. et al., 2018, A&A, 614, A3
Rebollido I. et al., 2022, MNRAS, 509, 693
Redfield S., Linsky J. L., 2002, ApJS, 139, 439
Redfield S., Linsky J. L., 2008, ApJ, 673, 283
Reffert S., Bergmann C., Quirrenbach A., Trifonov T., Künstler A., 2015, A&A, 574, A116
Ribas Á., Bouy H., Merín B., 2015, A&A, 576, A52
Riviere-Marichalar P. et al., 2014, A&A, 565, A68
Roberge A., Feldman P. D., Lagrange A. M., Vidal-Madjar A., Ferlet R., Jolly A., Lemaire J. L., Rostas F., 2000, ApJ, 538, 904
Schneiderman T. et al., 2021, Nature, 598, 425
Smette A. et al., 2015, A&A, 576, A77
Smirnov-Pinchukov G. V., Moór A., Semenov D. A., Ábrahám P., Henning T., Kóspál Á., Hughes A. M., di Folco E., 2022, MNRAS, 510, 1148
Somerville W. B., 1988, Observatory, 108, 44
Szewczyk K. M., Panić O., Iglesias D. P., Pearce T. D., Miley J. M., 2025, MNRAS, p. 545 staf2150
Taylor M. B., 2005, in Shopbell P., Britton M., Ebert R., eds, ASP Conf. Ser. Vol. 347, Astronomical Data Analysis Software and Systems XIV. Astron. Soc. Pac., San Francisco, p. 29
Veras D., Tremblay P.-E., Hermes J. J., McDonald C. H., Kennedy G. M., Meru F., Gänsicke B. T., 2020, MNRAS, 493, 765
Welsh B. Y., Montgomery S., 2013, PASP, 125, 759
Welsh B. Y., Montgomery S. L., 2015, Adv. Astron., 2015, 1
Welsh B. Y., Montgomery S. L., 2018, MNRAS, 474, 1515
Welsh B. Y., Craig N., Crawford I. A., Price R. J., 1998, A&A, 338, 674
Wenger M. et al., 2000, A&AS, 143, 9
Wyatt M. C., 2008, ARA&A, 46, 339
Wyatt M. C., Panić O., Kennedy G. M., Matrà L., 2015, Ap&SS, 357, 103

APPENDIX A: ORIGIN OF NARROW ABSORPTION FEATURES IN FULL SAMPLE

Table A1. List of 130 objects from the D. P. Iglesias et al. (2023a) sample used in this study, showing whether or not they have narrow absorption features in the Ca II K line and how many, and if we consider them circumstellar or interstellar in nature. For parameters of these objects, see the aforementioned study. Possible MS stars are marked with ^{MS}.

Name	Number of absorption features	Absorption feature origin	Name	Number of absorption features	Absorption feature origin
HIP 102719	1	Interstellar	HIP 79878	1	Interstellar
HIP 105148	1	Interstellar	HIP 80387	1	Interstellar
HIP 107962	1	Interstellar	HIP 80477	0	–
HIP 115551	1	Interstellar	HIP 81045	1	Interstellar
HIP 12055	2	Interstellar	HIP 81474	0	–
HIP 13910	1	Interstellar	HIP 81891	2	Interstellar
HIP 17543	1	Interstellar	HIP 82091	0	–
HIP 21024	2	Interstellar	HIP 82154	1	Interstellar
HIP 22370	3	Interstellar	HIP 82173	1	Interstellar
HIP 22402	1	Interstellar	HIP 82714	1	Interstellar
HIP 23633	1	Interstellar	HIP 83505	2	Interstellar
HIP 24092	1	Interstellar	HIP 84175	2	Interstellar
HIP 25453	1	Interstellar	HIP 84628	1	Interstellar
HIP 25763	1	Interstellar	HIP 85372	0	–
HIP 25998	0	–	HIP 86429	1	Interstellar
HIP 26783	1	Interstellar	HIP 87807	2	Interstellar
HIP 28877	3	Interstellar	HIP 89114	0	–
HIP 30054	4	Interstellar	HIP 90609	3	Interstellar
HIP 30353	2	Interstellar	HIP 91779	1	Interstellar
HIP 30414	Variable features	Possibly circumstellar	HIP 91893	1	Interstellar
HIP 30672	3	Interstellar	HIP 92188	1	Interstellar
HIP 32667	2	Interstellar	HIP 92800	1	Interstellar
HIP 32731	2	Interstellar	HIP 93525	1	Interstellar
HIP 36225	1	Interstellar	HIP 93542	1	Interstellar
HIP 36966	1	Interstellar	HIP 93744	0	–
HIP 37094	1	Interstellar	HIP 94167	2	Interstellar
HIP 37697	1	Interstellar	HIP 94949	2	Interstellar
HIP 40594	1	Interstellar	HIP 95547	1	Interstellar
HIP 43643	1	Interstellar	HIP 95619	2	Interstellar
HIP 45585	1	Interstellar	HIP 95979	2	Interstellar
HIP 48613	3	Interstellar	TYC 1019-473-1^{MS}	0	–
HIP 49606	1	Interstellar	TYC 1302-69-1	3	Interstellar
HIP 51843	1	Interstellar	TYC 1600-168-1	2	Interstellar

Downloaded from https://academic.oup.com/mnras/article/550/4/stag1309/8732235 by guest on 31 July 2026

Table A1 – *continued*

Name	Number of absorption features	Absorption feature origin	Name	Number of absorption features	Absorption feature origin
HIP 52688	1	Interstellar	TYC 1765-1373-1	1	Interstellar
HIP 56943	2	Interstellar	TYC 2138-1154-1	0	–
HIP 57027	0	–	TYC 2140-893-1^{MS}	2	Interstellar
HIP 58720	1	Interstellar	TYC 435-302-1	2	Interstellar
HIP 59898	1	Interstellar	TYC 457-39-1	1	Interstellar
HIP 60183	1	Interstellar	TYC 4822-542-1	1	Interstellar
HIP 60561	1	Interstellar	TYC 5124-2609-1	2	Interstellar
HIP 61498	2	Interstellar	TYC 5597-720-1	1	Interstellar
HIP 61782^{MS}	2	Circumstellar	TYC 5649-822-1	3	Interstellar
HIP 63839	0	–	TYC 6487-537-1	1	Interstellar
HIP 66068	1	Interstellar	TYC 6822-283-1	5	Inconclusive
HIP 69011	1	Interstellar	TYC 6843-956-1	1	Interstellar
HIP 69761	1	Interstellar	TYC 6846-840-1	1	Interstellar
HIP 70040	1	Interstellar	TYC 6849-1024-1	1	Interstellar
HIP 73150	1	Interstellar	TYC 6849-1059-1	1	Interstellar
HIP 73397^{MS}	1	Interstellar	TYC 7374-702-1	1	Interstellar
HIP 75210	2	Interstellar	TYC 7379-170-1	1	Interstellar
HIP 75902	1	Interstellar	TYC 7389-385-1	1	Interstellar
HIP 76011	1	Interstellar	TYC 7645-1683-1	2	Interstellar
HIP 76234	4	Interstellar	TYC 7851-91-1	2	Interstellar
HIP 76244	1	Interstellar	TYC 7879-1373-1	3	Possibly circumstellar
HIP 76310	1	Interstellar	TYC 7879-1506-1	1	Interstellar
HIP 76395	1	Interstellar	TYC 7892-4279-1	0	–
HIP 77315	0	–	TYC 8161-658-1	1	Interstellar
HIP 77317	0	–	TYC 8241-3236-1	1	Interstellar
HIP 77562	1	Interstellar	TYC 8603-1782-1	1	Interstellar
HIP 77911	1	Interstellar	TYC 8697-1251-1	0	–
HIP 79179	1	Interstellar	TYC 8703-571-1	1	Interstellar
TYC 8946-1580-1	1	Interstellar			
TYC 8959-774-1	1	Interstellar			
TYC 8977-9252-1	1	Interstellar			
TYC 8995-1696-1	1	Interstellar			
TYC 9004-2647-1	1	Interstellar			
TYC 9005-873-1	1	Interstellar			
TYC 9009-1874-1	1	Interstellar			
TYC 9329-60-1	1	Interstellar			

APPENDIX B: OBSERVATIONS

Downloaded from https://academic.oup.com/mnras/article/550/4/stag1309/8732235 by guest on 31 July 2026

Table B1. Observation details for the 130 objects analysed in this study. The columns include: object name used in this study, HD identifier (if available), coordinates, instruments used for observations, number of observations, observation dates, and signal-to-noise ratio (maximum value if multiple epochs are available).

Name	HD identifier	RA	Dec.	Instrument	Number of spectra	Observation dates	S/N
HIP 102719	HD 197827	20:48:50.68	−59:14:04.0	UVES	6	2022-07-10 to 2022-08-22	160
HIP 105148	HD 202299	21:18:00.49	−64:40:53.7	FEROS	1	2007-05-25 to 2007-05-25	359
HIP 107962	HD 207888	21:52:21.25	−03:10:28.8	UVES	4	2022-05-11 to 2022-07-05	191
HIP 115551	HD 220529	23:24:21.80	+06:11:10.6	UVES	4	2022-07-05 to 2022-08-23	170
HIP 12055	HD 16152	02:35:24.47	−09:21:02.7	UVES	4	2022-07-05 to 2022-08-23	129
HIP 13910	HD 18572	02:59:08.41	−04:47:00.1	UVES	4	2022-09-01 to 2022-09-11	123
HIP 17543	HD 24188	03:45:23.74	−71:39:29.3	UVES	6	2023-09-13 to 2023-09-15	323
HIP 21024	HD 28813	04:30:29.54	−43:24:38.2	UVES	8	2023-09-13 to 2024-02-02	274
HIP 22370	HD 30861	04:48:57.47	−47:08:04.3	UVES	6	2022-07-24 to 2022-08-23	139
HIP 22402	HD 30466	04:49:16.01	+29:34:16.8	UVES	6	2023-09-20 to 2023-09-23	249
HIP 23633	HD 32509	05:04:50.13	+26:43:14.8	UVES	6	2023-09-20 to 2023-10-11	238
HIP 24092	HD 33594	05:10:32.96	−18:39:44.8	UVES	4	2022-09-01 to 2022-09-09	116
HIP 25453	HD 35656	05:26:38.83	+06:52:07.2	UVES	2	2022-09-23 to 2022-09-23	157
HIP 25763	HD 36044C	05:30:05.99	+29:33:10.1	UVES	12	2023-10-11 to 2023-10-16	356
HIP 25998	HD 37004	05:32:56.39	−47:41:20.9	UVES	6	2022-07-24 to 2022-09-09	127
HIP 26783	HD 37647	05:41:21.47	+29:29:39.9	UVES	6	2023-10-11 to 2023-10-12	314
HIP 28877	HD 41649	06:05:48.33	−16:57:33.8	UVES	6	2023-09-13 to 2023-09-27	206
HIP 30054	HD 44405	06:19:28.47	−42:53:10.9	UVES	6	2023-09-13 to 2023-09-17	201
HIP 30353	HD 44618	06:23:05.33	+10:10:03.7	UVES	6	2023-09-21 to 2023-09-29	241
HIP 30414	HD 44892	06:23:42.76	−16:28:01.9	UVES	6	2023-09-13 to 2023-09-27	291
HIP 30672	HD 45681	06:26:43.63	−44:04:02.9	UVES	4	2022-10-20 to 2022-12-06	213
HIP 32667	HD 49610	06:48:49.30	−08:18:36.9	UVES	6	2023-10-16 to 2023-11-01	255
HIP 32731	HD 49812	06:49:40.11	−15:02:40.5	UVES	5	2022-12-29 to 2023-10-16	246
HIP 36225	HD 59074	07:27:34.48	−18:29:30.8	UVES	6	2023-10-16 to 2023-11-01	266
HIP 36966	HD 60875	07:35:56.95	−18:50:47.0	UVES	6	2023-10-16 to 2023-11-11	391
HIP 37094	HD 61308	07:37:20.03	−30:47:32.0	UVES	9	2023-10-16 to 2023-10-30	259
HIP 37697	HD 62803	07:44:02.50	−38:49:04.6	UVES	6	2022-09-08 to 2022-09-19	149
HIP 40594	HD 69952	08:17:16.65	−46:53:35.7	UVES	2	2022-09-14 to 2022-09-14	138
HIP 43643	HD 76268	08:53:22.31	−44:19:59.2	UVES	2	2022-09-25 to 2022-09-25	176
HIP 45585	HD 80950	09:17:27.57	−74:44:04.5	HARPS	28	2012-02-19 to 2012-05-03	175
HIP 48613	HD 86087	09:54:51.23	−50:14:38.3	FEROS	2	2016-01-03 to 2016-01-04	306
				HARPS	21	2018-12-19 to 2019-07-19	385
				UVES	2	2019-01-24 to 2019-01-24	232
HIP 49606	HD 88068	10:07:31.00	−57:32:59.8	UVES	6	2023-10-16 to 2023-11-13	423
HIP 51843	HD 92047	10:35:30.32	−69:49:02.8	UVES	4	2022-06-11 to 2022-07-09	127
HIP 52688	HD 93331	10:46:24.83	−13:27:35.5	UVES	6	2023-11-22 to 2023-11-30	267
HIP 56943	HD 101511	11:40:26.42	−62:11:53.8	UVES	2	2022-07-10 to 2022-07-10	153
HIP 57027	HD 101727	11:41:32.57	−77:03:16.9	UVES	2	2022-07-10 to 2022-07-10	199
HIP 58720	HD 104600	12:02:37.69	−69:11:32.2	UVES	6	2017-02-22 to 2019-02-21	239
HIP 59898	HD 106797	12:17:06.31	−65:41:34.7	UVES	6	2017-02-22 to 2019-02-21	289
HIP 60183	HD 107301	12:20:28.22	−65:50:33.6	UVES	6	2017-02-22 to 2019-02-21	261
HIP 60561	HD 107947	12:24:51.92	−72:36:14.0	UVES	8	2018-12-24 to 2018-12-28	284
HIP 61498	HD 109573	12:36:01.03	−39:52:10.2	FEROS	29	2007-03-09 to 2017-04-09	492
				HARPS	10	2007-12-06 to 2015-01-21	313
				UVES	486	2002-01-19 to 2007-05-15	523
HIP 61782	HD 110058	12:39:46.20	−49:11:55.6	FEROS	11	2010-01-31 to 2017-04-09	329
				HARPS	15	2015-01-18 to 2018-03-31	205
HIP 63839	HD 113457	13:05:02.04	−64:26:29.7	UVES	6	2017-03-20 to 2019-02-20	358
HIP 66068	HD 117665	13:32:39.24	−44:27:00.9	UVES	6	2019-01-24 to 2019-02-21	251
HIP 69011	HD 123247	14:07:40.81	−48:42:14.5	UVES	6	2023-12-20 to 2023-12-27	208
HIP 69761	HD 124564	14:16:37.50	−62:06:59.4	UVES	4	2022-05-26 to 2022-07-10	221
HIP 70040	HD 125205	14:19:54.59	−57:09:27.3	UVES	6	2023-12-28 to 2023-12-31	181
HIP 73150	HD 131885	14:56:57.45	−26:17:06.1	UVES	4	2022-05-26 to 2022-07-13	189
HIP 73397	HD 132658	14:59:59.53	+12:01:26.2	UVES	4	2022-08-05 to 2022-08-22	163
HIP 75210	HD 136482	15:22:11.25	−37:38:08.2	HARPS	1	2015-01-19 to 2015-01-19	192
				UVES	4	2017-03-20 to 2019-02-24	322
HIP 75902	HD 137641	15:30:11.59	−60:29:27.2	UVES	4	2022-07-10 to 2022-08-10	138
HIP 76011	HD 137509	15:31:27.11	−71:03:43.7	UVES	6	2001-07-12 to 2008-04-17	175
HIP 76234	HD 138564	15:34:20.85	−39:20:57.1	UVES	6	2023-09-26 to 2024-01-11	215
HIP 76244	HD 138334	15:34:26.59	−59:48:03.4	UVES	4	2022-06-11 to 2022-07-10	137
HIP 76310	HD 138813	15:35:16.11	−25:44:03.0	FEROS	13	2016-03-26 to 2017-04-08	389
				UVES	6	2016-02-22 to 2016-03-18	181

Downloaded from https://academic.oup.com/mnras/article/550/4/stag1309/8732235 by guest on 31 July 2026

Table B1 – *continued*

Name	HD identifier	RA	Dec.	Instrument	Number of spectra	Observation dates	S/N
HIP 76395	HD 138923	15:36:11.36	−33:05:34.1	FEROS	2	2009-02-06 to 2009-02-06	233
				UVES	6	2019-01-26 to 2019-02-22	253
HIP 77315	HD 140817	15:47:04.46	−35:30:37.2	FEROS	2	2009-07-20 to 2009-07-20	210
				UVES	6	2019-02-24 to 2019-03-10	336
HIP 77317	HD 140840	15:47:06.17	−35:31:04.9	FEROS	2	2009-02-06 to 2009-02-06	213
				UVES	1	2016-02-21 to 2016-02-21	126
HIP 77562	HD 141168	15:50:07.08	−53:12:35.2	UVES	4	2022-07-10 to 2022-07-13	187
HIP 77911	HD 142315	15:54:41.60	−22:45:58.5	FEROS	5	2010-02-01 to 2017-04-05	333
HIP 79179	HD 144696	16:09:38.67	−52:06:55.1	UVES	4	2022-07-13 to 2022-07-23	186
HIP 79878	HD 146606	16:18:16.16	−28:02:30.1	FEROS	5	2009-07-20 to 2017-04-09	309
				UVES	2	2016-09-12 to 2016-09-12	220
HIP 80387	HD 147703	16:24:30.43	−27:09:04.2	UVES	4	2022-07-13 to 2022-07-23	162
HIP 80477	HD 148021	16:25:38.21	−10:05:02.8	UVES	6	2023-09-23 to 2024-01-31	213
HIP 81045	HD 148850	16:33:11.00	−47:41:00.2	UVES	4	2022-07-13 to 2022-07-23	214
HIP 81474	HD 149914	16:38:28.65	−18:13:13.7	UVES	6	2023-09-17 to 2023-09-30	278
HIP 81891	HD 150638	16:43:38.72	−32:06:21.4	UVES	6	2023-09-14 to 2023-09-17	217
HIP 82091	HD 150897	16:46:06.37	−46:31:55.2	UVES	4	2022-07-13 to 2022-07-25	181
HIP 82154	HD 151109	16:47:01.68	−39:32:01.9	FEROS	2	2007-04-01 to 2017-07-19	359
				UVES	4	2016-10-01 to 2016-10-01	287
HIP 82173	HD 150915	16:47:19.90	−57:27:38.9	UVES	5	2022-07-25 to 2022-08-14	181
HIP 82714	HD 152384	16:54:26.39	−33:28:31.3	UVES	6	2022-07-14 to 2022-07-25	162
HIP 83505	HD 154002	17:03:59.08	−28:15:22.7	FEROS	1	2008-04-01 to 2008-04-01	233
				UVES	4	2022-06-24 to 2022-07-14	115
HIP 84175	HD 155401	17:12:25.06	−27:45:43.7	UVES	6	2022-07-14 to 2022-07-25	189
HIP 84628	HD 156157	17:18:01.37	−43:34:39.7	UVES	8	2022-07-09 to 2022-07-23	196
HIP 85372	HD 157751	17:26:41.19	−34:05:32.5	HARPS	3	2007-04-15 to 2007-04-15	171
HIP 86429	HD 160047	17:39:34.62	−38:23:44.5	UVES	4	2023-03-11 to 2023-03-23	240
HIP 87807	HD 163422	17:56:15.03	−04:34:35.0	UVES	6	2023-09-14 to 2023-09-15	276
HIP 89114	HD 166393	18:11:14.78	−19:50:31.0	UVES	6	2022-07-17 to 2022-08-11	156
HIP 90609	HD 170562	18:29:20.86	+17:59:02.1	UVES	6	2023-09-14 to 2023-09-16	196
HIP 91779	HD 173054	18:42:54.22	+13:34:00.2	UVES	4	2022-08-10 to 2022-08-11	141
HIP 91893	HD 173196	18:43:59.29	+03:20:38.2	UVES	4	2022-08-06 to 2022-08-10	135
HIP 92188	HD 173505	18:47:19.04	−37:32:55.2	FEROS	1	2019-08-01 to 2019-08-01	90
				UVES	4	2014-04-27 to 2014-04-27	184
HIP 92800	HD 175427	18:54:32.85	+20:36:55.1	UVES	6	2023-09-14 to 2023-09-16	188
HIP 93525	HD 177064	19:02:53.62	+05:20:33.9	UVES	4	2022-08-19 to 2022-08-21	151
HIP 93542	HD 176638	19:03:06.88	−42:05:42.4	FEROS	2	2009-06-02 to 2010-05-26	405
				HARPS	10	2005-08-20 to 2006-05-25	273
HIP 93744	HD 177625	19:05:20.03	+05:53:37.6	UVES	4	2022-08-06 to 2022-08-10	191
HIP 94167	HD 178857	19:10:07.28	+00:55:55.2	UVES	4	2022-08-06 to 2022-08-14	170
HIP 94949	HD 181253	19:19:17.01	+14:10:39.3	UVES	6	2023-09-14 to 2023-09-16	321
HIP 95547	HD 182740	19:26:05.13	+03:31:09.7	UVES	4	2022-08-11 to 2022-08-14	152
HIP 95619	HD 182681	19:26:56.48	−29:44:35.6	UVES	6	2023-09-13 to 2023-09-14	257
HIP 95979	HD 182254	19:31:01.04	−73:59:06.8	UVES	6	2022-07-09 to 2022-07-13	183
TYC 1019-473-1	HD 162951	17:53:08.80	+14:00:34.9	UVES	4	2022-08-11 to 2022-08-26	232
TYC 1302-69-1	HD 37673	05:41:08.87	+18:37:28.0	UVES	6	2023-10-12 to 2023-10-16	258
TYC 1600-168-1	HD 182445	19:24:03.98	+15:43:46.5	UVES	4	2022-08-06 to 2022-08-10	123
TYC 1765-1373-1	-	02:21:36.14	+23:37:54.7	UVES	12	2023-09-13 to 2023-09-14	232
TYC 2138-1154-1	HD 344687	19:39:26.96	+23:52:48.0	UVES	4	2022-08-10 to 2022-08-19	189
TYC 2140-893-1	HD 345089	19:52:03.18	+23:26:21.1	UVES	4	2022-08-10 to 2022-08-13	159
TYC 365-704-1	HD 142537	15:56:36.40	−42:19:33.8	FEROS	1	2008-06-16 to 2008-06-16	395
TYC 435-302-1	HD 167392	18:14:52.60	+03:40:23.3	UVES	4	2022-08-10 to 2022-08-11	141
TYC 457-39-1	HD 176305	18:59:25.67	+05:15:03.5	UVES	4	2022-08-10 to 2022-08-22	143
TYC 4703-768-1	HD 18572	02:59:08.41	−04:47:00.1	UVES	4	2022-09-01 to 2022-09-11	123
TYC 4822-542-1	HD 52208	07:00:09.45	−05:22:41.8	UVES	6	2023-10-02 to 2023-10-16	243
TYC 5091-298-1	HD 163422	17:56:15.03	−04:34:35.0	UVES	6	2023-09-14 to 2023-09-15	276
TYC 5124-2609-1	HD 171837	18:37:14.68	−06:36:17.8	UVES	12	2023-09-13 to 2023-09-15	315
TYC 5597-720-1	HD 140541	15:44:30.83	−09:13:55.0	UVES	4	2023-02-28 to 2023-03-20	246
TYC 5649-822-1	HD 156267	17:17:02.17	−10:39:42.3	UVES	4	2022-08-06 to 2022-08-09	129
TYC 5905-1186-1	HD 33594	05:10:32.96	−18:39:44.8	UVES	4	2022-09-01 to 2022-09-09	116
TYC 6487-537-1	-	05:20:35.61	−29:43:29.0	UVES	12	2023-09-13 to 2023-09-17	250

Downloaded from https://academic.oup.com/mnras/article/550/4/stag1309/8732235 by guest on 31 July 2026

Table B1 – *continued*

Name	HD identifier	RA	Dec.	Instrument	Number of spectra	Observation dates	S/N
TYC 6822-283-1	HD 152519	16:55:00.67	−29:51:10.2	UVES	6	2022-07-14 to 2022-07-25	165
TYC 6843-956-1	HD 165999	18:09:36.27	−23:34:04.7	UVES	5	2023-03-11 to 2023-09-14	233
TYC 6846-840-1	HD 164147	18:00:50.96	−24:47:18.7	UVES	6	2022-06-24 to 2022-08-26	190
TYC 6849-1024-1	HD 314750	17:53:04.53	−27:00:12.7	UVES	4	2022-06-24 to 2022-07-23	162
TYC 6849-1059-1	HD 162655	17:53:16.77	−27:37:44.3	UVES	4	2022-06-24 to 2022-07-10	124
TYC 7374-702-1	HD 157036	17:22:31.48	−36:30:49.6	UVES	6	2022-07-14 to 2022-07-25	153
TYC 7379-170-1	HD 158422	17:30:40.21	−32:03:42.3	UVES	4	2022-06-24 to 2022-07-14	110
TYC 7389-385-1	HD 161759	17:48:59.86	−37:17:42.8	UVES	4	2022-06-24 to 2022-07-09	151
TYC 7645-1683-1	HD 62938	07:44:44.89	−38:03:13.4	UVES	4	2022-09-14 to 2022-09-20	147
TYC 7851-91-1	HD 143181	16:00:22.34	−38:59:37.7	UVES	4	2022-07-13 to 2022-07-23	160
TYC 7879-1373-1	HD 151183	16:47:47.43	−43:56:18.1	UVES	4	2022-07-13 to 2022-07-22	148
TYC 7879-1506-1	HD 150477	16:43:11.25	−43:39:10.4	UVES	4	2022-07-13 to 2022-07-23	166
TYC 7892-4279-1	HD 159807	17:38:36.75	−42:44:01.9	UVES	4	2022-06-24 to 2022-07-10	154
TYC 8161-658-1	HD 70702	08:21:00.82	−51:32:36.9	FEROS	1	2007-02-10 to 2007-02-10	123
TYC 8241-3236-1	HD 105383	12:08:04.87	−50:45:49.1	UVES	2	2022-07-10 to 2022-07-10	144
TYC 8603-1782-1	HD 87322	10:02:31.48	−56:12:22.9	UVES	2	2022-07-09 to 2022-07-09	143
TYC 8697-1251-1	HD 142564	15:57:51.79	−53:45:27.1	UVES	4	2022-07-10 to 2022-07-13	143
TYC 8703-571-1	HD 136155	15:21:34.13	−56:54:07.3	UVES	4	2022-07-10 to 2022-07-23	171
TYC 8946-1580-1	HD 86836	09:58:57.89	−62:19:00.2	UVES	2	2022-07-09 to 2022-07-09	156
TYC 8959-774-1	HD 97558	11:12:38.20	−60:55:16.1	UVES	2	2022-07-10 to 2022-07-10	105
TYC 8977-9252-1	HD 103457	11:54:32.75	−63:42:02.2	UVES	2	2022-07-10 to 2022-07-10	155
TYC 8995-1696-1	HD 117959	13:35:26.97	−61:57:09.3	UVES	4	2022-05-30 to 2022-07-09	121
TYC 9004-2647-1	HD 121808	13:59:40.59	−61:22:52.5	UVES	4	2022-05-30 to 2022-07-09	129
TYC 9005-873-1	HD 124340	14:15:09.92	−61:06:42.1	UVES	4	2022-07-09 to 2022-08-10	127
TYC 9009-1874-1	HD 122965	14:07:05.94	−62:16:38.0	UVES	4	2022-05-26 to 2022-05-30	190
TYC 9329-60-1	HD 198147	20:53:24.09	−71:50:13.9	UVES	12	2023-09-13 to 2023-09-14	241

Downloaded from https://academic.oup.com/mnras/article/550/4/stag1309/8732235 by guest on 31 July 2026

Table B2. Observation details for the additional 38 objects used as comparison stars in this study. The columns include: object name used in this study, coordinates, instruments used for observations, number of observations, observation dates, and signal-to-noise ratio (maximum value if multiple epochs are available).

Name	RA	Dec.	Instrument	Number of spectra	Observation dates	S/N
BD-07 534	12:20:11.44	−53:05:22.4	UVES	2	2024-08-12	364
HD 101638	19:49:3.71	−09:04:22.6	UVES	2	2024-05-22	302
HD 101671	19:40:5.71	+00:58:14.8	UVES	2	2024-05-21	226
HD 117337	20:41:13.50	+18:26:18.9	UVES	2	2024-05-20	368
HD 121720	20:43:31.22	+00:12:52.3	UVES	2	2024-05-22	356
HD 131369	22:16:36.73	+28:36:33.9	UVES	2	2024-06-22	150
HD 132446	00:49:55.89	+56:34:24.1	UVES	2	2024-08-17	374
HD 136423	22:12:49.75	+16:19:33.1	UVES	2	2024-06-08	238
HD 137927	21:03:54.25	−11:27:48.5	UVES	2	2024-05-23	265
HD 138871	22:54:47.15	+24:26:32.9	UVES	2	2024-06-22	239
HD 141705	21:54:48.95	+01:13:48.9	UVES	2	2024-06-22	446
HD 142220	21:53:37.45	+00:08:17.3	UVES	2	2024-06-22	264
HD 142705	23:16:9.95	+22:39:43.6	UVES	2	2024-04-03	348
HD 150990	22:56:17.69	+03:38:41.5	UVES	4	2024-07-31 to 2024-08-02	306
HD 152192	23:28:57.20	+08:30:12.5	UVES	2	2024-07-31	360
HD 156248	00:47:13.16	+15:18:6.8	UVES	2	2024-08-17	429
HD 15657	11:53:52.89	−59:39:31.9	UVES	2	2024-06-27	149
HD 156622	23:00:46.30	−03:36:36.2	UVES	2	2024-06-09	206
HD 163799	00:28:39.52	+00:45:32.8	UVES	2	2024-08-03	314
HD 167307	02:08:22.55	+09:56:11.3	UVES	2	2024-08-11	247
HD 173891	23:57:4.40	−15:24:7.2	UVES	2	2024-06-28	277
HD 176425	23:40:8.38	−19:36:11.9	UVES	2	2024-05-06	278
HD 178953	02:22:55.10	−03:56:10.2	UVES	2	2024-06-28	246
HD 182621	02:39:34.24	−05:59:19.04	UVES	2	2024-06-28	200
HD 198534	22:26:28.46	−38:28:6.5	UVES	2	2024-06-27	158
HD 221272	05:55:19.45	−52:11:35.1	UVES	2	2024-08-01	295
HD 230787	03:13:57.66	+02:58:56.4	UVES	2	2024-08-12	286
HD 29929	16:45:35.95	−41:25:50.3	UVES	2	2024-07-24	329
HD 307428	18:54:43.42	−05:41:15.7	UVES	2	2024-05-22	227
HD 345199	04:01:37.43	−02:12:27.4	UVES	2	2024-05-20	297
HD 35714	13:05:45.69	−15:08:9.1	UVES	2	2024-08-12	310
HD 70007	17:33:20.49	−06:23:16.5	UVES	2	2024-05-23	75
HD 76516	17:38:44.44	+00:47:52.8	UVES	2	2024-05-22	260
HD 80951	19:20:56.60	−17:35:41.5	UVES	2	2024-05-21	178
HD 87122	18:43:3.71	+00:43:59.9	UVES	2	2024-05-18	262
HD 92316	19:28:21.60	−10:26:16.6	UVES	2	2024-05-21	207
V∗ IN Lup	22:33:35.06	+10:52:3.5	UVES	2	2024-07-31	476
V∗ KN Vel	18:21:25.53	+02:49:49.4	UVES	2	2024-05-21	189

APPENDIX C: PHOTOSPHERE FITS

Downloaded from https://academic.oup.com/mnras/article/550/4/stag1309/8732235 by guest on 31 July 2026

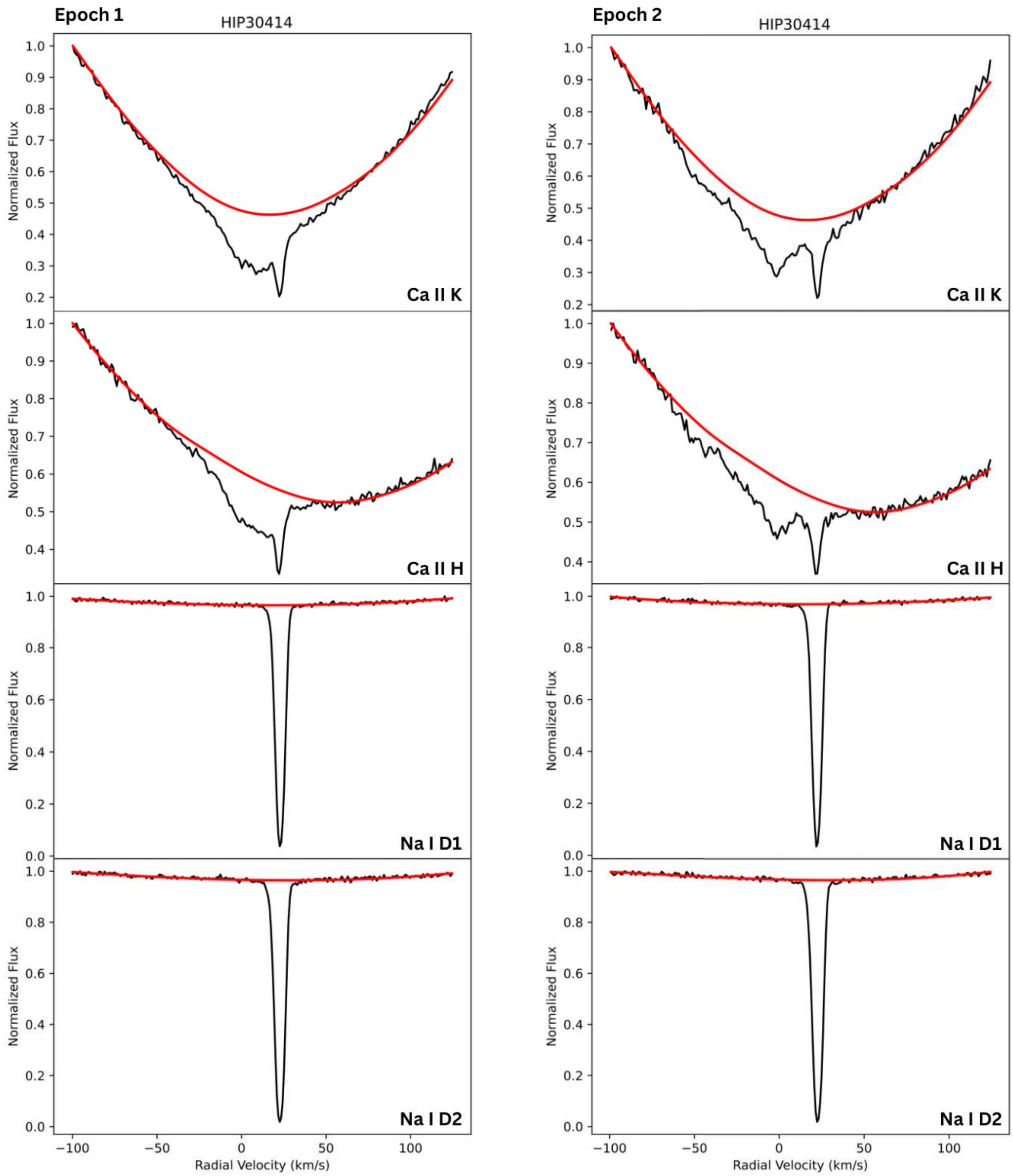

Figure C1. Photospheric spectrum of HIP 30414 in Ca II K & H and Na I D1 & D2 lines. Columns are two different epochs we observed, showing variability between them. Black line is the flux, while red curve is the fitted Kurucz photosphere model used to isolate narrow features. The model parameters for Ca II K are: temperature 7440 K, log(g) 4.2, [Fe/H] 0, $v$sin(i) 130 km s^{-1}; for Ca II H: temperature 7400 K, log(g) 4.2, [Fe/H] 0, $v$sin(i) 135 km s^{-1}.

Downloaded from https://academic.oup.com/mnras/article/550/4/stag1309/8732235 by guest on 31 July 2026

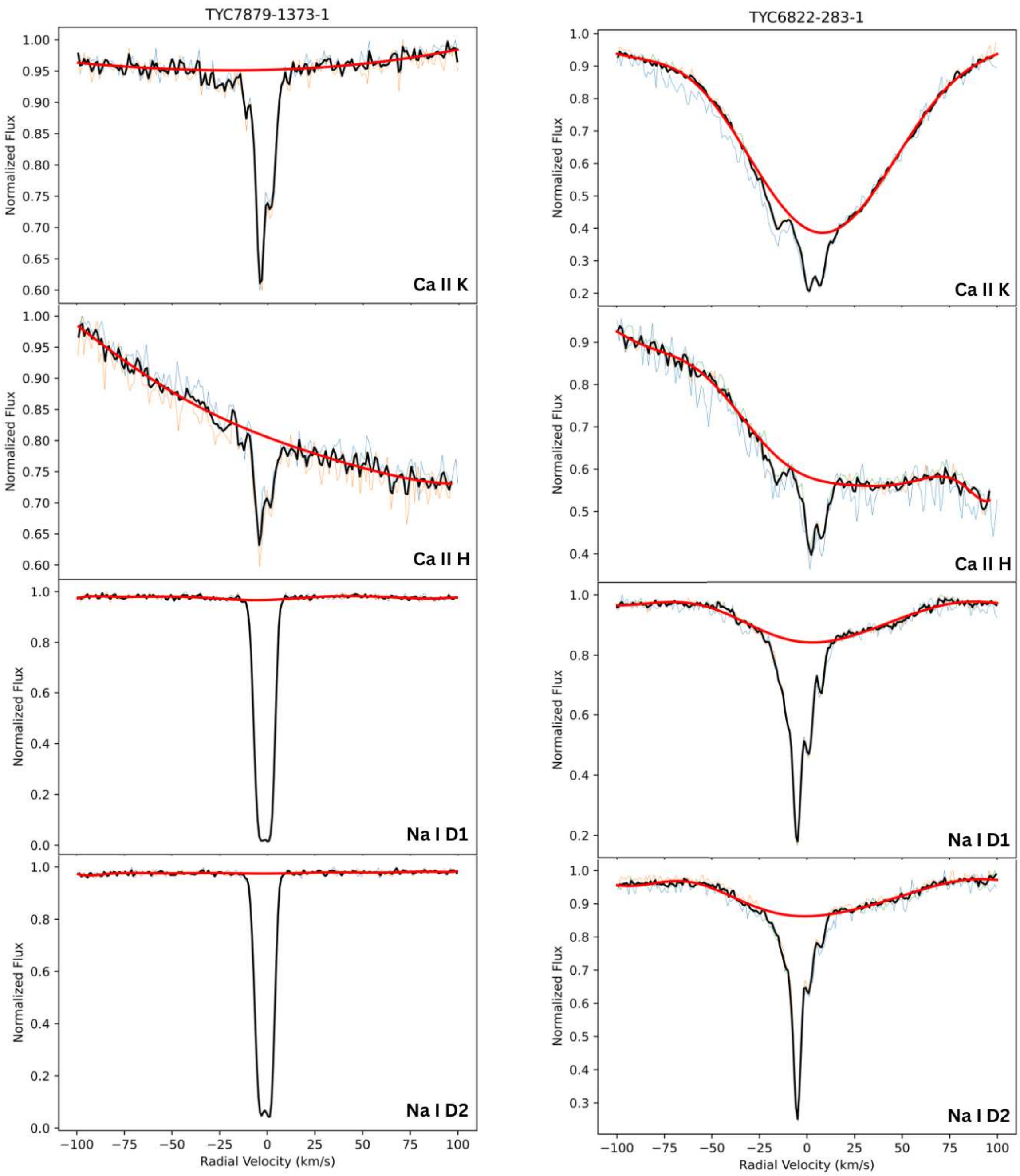

Figure C2. **Left:** Photospheric spectrum of TYC 7879-1373-1, in Ca II K & H and Na I D1 & D2 lines, as normalized flux vs radial velocity [km s^{-1}]. Black line is the median flux of all epochs, while red curve is the photospheric absorption fitted with a polynomial used to isolate narrow features. **Right:** Same but for TYC 6822-283-1.

This paper has been typeset from a TEX/LATEX file prepared by the author.

© The Author(s) 2026.
Published by Oxford University Press on behalf of Royal Astronomical Society. This is an Open Access article distributed under the terms of the Creative Commons Attribution License (https://creativecommons.org/licenses/by/4.0/), which permits unrestricted reuse, distribution, and reproduction in any medium, provided the original work is properly cited.

Downloaded from https://academic.oup.com/mnras/article/550/4/stag1309/8732235 by guest on 31 July 2026